Preparation of high-concentration charged solutions through dual electrostatic method for ice crystals and desalination

Zhongzheng MIAO[1, 2 *]

[1] School of Physics and Electronic Engineering, Yancheng Teachers University, Yancheng 224007, China

[2] Yancheng Meiheng Science & Technology Co., Ltd, Yancheng 224007, China

Zhongzheng Miao contributed all content

[*] Corresponding author: Zhongzheng Miao (E-mail: miaozz@yctu.edu.cn)

Abstract

Under typical circumstances, it is commonly believed that solutions carrying a single type of charge are either non-existent or unstable. We have investigated the principles of high-concentration charged solution preparation techniques, employing methods such as electrostatic attraction, gravity separation, positive feedback, and self-powered mechanisms to effectively separate anions and cations in solution. Through electrostatic repulsion and the use of electrostatic separation networks, the partition of homoelectric ions has been achieved. Through water and electric separation, the capability for sustained accumulation of single-charge species has been attained, thus overcoming application bottlenecks and establishing evidence for the existence of charged solutions. We have proposed voltage limits and predicted phenomena such as electrostatic boiling, topological ice crystals, and strange ice crystals, thereby opening new perspectives and possibilities for enriching the understanding and research of electrostatics and electrochemistry. The introduction of the high-concentration charged solution and its controllable preparation are expected to facilitate or pioneer research in various fields including seawater desalination, wastewater treatment, hydrovoltaic power generation, and topological ice crystals, etc. This advancement holds the potential to rectify relevant discussions in textbooks. Implementing the dual electrostatic method for self-powered desalination and purification, coupled with wind, solar, and pumped hydro storage technologies, can aid in mitigating the intermittency and waste of wind and solar power, thus advancing the cause of seawater for land.

Keywords: Dual electrostatic method; Charged solution; Topological ice crystal; Desalination and water purification; Electrostatic boiling

1. Introduction

Generally, it is believed that solutions with a single type (net) charge are either nonexistent or unstable. The question of whether a glass of water can bear a voltage of tens of thousands of volts, and how to induce a glass of water to possess such high voltage, along with its macroscopic and microscopic states, is rarely addressed. Research on high-concentration charged solutions currently remains unexplored: (1) The existence of charged solutions/high-concentration charged solutions; (2) Methods for preparing high-concentration charged solutions; (3) The distribution status and specific properties of ions/charges/charged particles in high-concentration charged solutions, including their storage limits and stability; (4) Application scenarios and technological principles of charged solutions. These four points constitute unresolved scientific questions. The introduction and controllable preparation of the high-concentration charged solution play a catalytic role in the theoretical research and practical application of electrostatics, electrochemistry, seawater desalination [1], wastewater treatment, nuclear wastewater treatment, hydrovoltaic power generation [2-10], frictional electricity [11], clean energy, water splitting, crystal preparation, strange metals, Hall effect, electrostatic boiling, topological ice crystals, etc. They may give rise to a series of related materials, devices, and apparatus for fundamental research and technological development, offering a plethora of application scenarios. This paper will propose and explore ten concepts: charged solutions, high-concentration charged solutions, charged ice crystals, topological ice crystals, conductive ice crystals, strange ice crystals, electrostatic boiling, anomalous Hall effect of dual-state charge carriers in equipotential body, self-powered desalination with dual electrostatic method, and seawater for land.

As human activities expand and environmental pollution worsens, the problem of clean water scarcity is becoming increasingly severe [12-14]. Water pollution is considered the most prominent issue in global public health challenges, with the situation growing more dire. Nearly one-third of the world's population cannot access clean drinking water. For example, in the coastal areas of Gaza, three desalination plants stopped production due to war-related power outages, leading to a more urgent and severe dehydration crisis than food scarcity for local residents. The World Health Organization reports that millions of children under the age of five die from diarrheal diseases each year, which are related to health issues such as ingesting unsafe water (heavy metal-charged ions) [15]. Nuclear wastewater typically contains large amounts of radioactive elements such as uranium,

plutonium, cesium, strontium, iodine, cobalt, etc., with high levels of radioactivity and danger, usually existing in dissolved charged forms. When desalinating seawater and extracting clean water, consideration should be given to removing these elements. Xu Xiao et al. conducted experiments using a laboratory-made vertical electric field electrophoresis device to study the desalination effect of simulated seawater. They investigated the effects of three factors—initial concentration of chloride ions (sodium chloride solution ranging from 466.4 to 862.0 mg/L), retention time (2-10.3 hours), and voltage (10-36 volts)—on desalination rate, energy efficiency, and distribution ratio, achieving a desalination rate of up to 69.5%. The positive feedback dual electrostatic method for self-powered desalination and clean water proposed in this paper has the following five advantages compared to traditional electrophoresis desalination methods: (1) External power sources such as power plants are non-essential options. With high voltage, it can provide stable voltages of 1-10 kilovolts or higher (without pursuing extreme high voltages). The desalination and clean water process can be implemented through metal containers, stainless steel mesh, conductors, etc., suitable for emergencies; (2) Easy modification. In the traditional electrophoresis desalination method, the coastal water intake method uses a water pump to directly pump water from the seaside, which is then transported to the factory area through a booster pump. Only the addition of a positive feedback loop is needed at the lower end of the traditional instrument outlet; (3) The traditional electrophoresis method only uses positive and negative electrodes to generate an electric field to directly treat seawater solutions containing positive and negative ions. The positive and negative ions in the solution have mutual attractive forces and tend to have uniform distribution without external forces. When a weak electric field force is applied, the desalination effect is not significant. When a strong electric field is applied, the mutual attractive force between positive and negative ions increases significantly, increasing the difficulty of separation and energy consumption. By comprehensively using the dual electrostatic method and positive feedback mechanism, separation is achieved through electrostatic attraction under the gravity of seawater, further achieving the separation of ion-containing water (pipe edge) and clean water (pipe center) based on the principle of electrostatic repulsion in the water and electric separation zone, reducing or avoiding the problem of uniform distribution caused by mutual attraction of positive and negative ions in the solution, thereby further improving the desalination rate of seawater; (4) Utilize wind power, photovoltaic technology, etc. to lift water and store energy, and prepare pure

water in situ on the sea; (5) This article implements the water-permeable power generation using stainless steel meshes, which contributes to the realization of potential energy's recovery and desalination for clean water, thereby advancing the exploration of seawater for land.

This article will initiate the exploration of the following research areas: charged solutions, high-concentration charged solutions, charged ice crystals, topological ice crystals, conductive ice crystals, strange ice crystals, electrostatic boiling, anomalous Hall effect of dual-state charge carriers in equipotential body, self-powered desalination with dual electrostatic method, and seawater for land. The application prospects of the research content in this article are as follows: (1) Desalination for clean water, seawater desalination, and nuclear wastewater treatment; (2) Hydrovoltaic power generation, sterilization, sensing and warning, rainwater utilization; (3) Absorption of abandoned wind and solar energy, in-situ production of clean water at sea, water supply for islands; (4) Preparation of CuCl crystals through the comproportionation reaction of Cu^{2+} and Cu; (5) Photolysis of water; (6) Providing new reaction pathways and raw materials for fields such as chemistry, biology, chemical engineering, and pharmaceuticals; (7) Preparation, properties, and applications of charged ice crystals, topological ice crystals, conductive ice crystals, strange ice crystals and even possibly providing inspiration for photolithography techniques.

2. Methodology and Design

This article uses the CASTEP software package based on density functional theory (DFT) using the first-principles plane-wave method. The exchange-correlation term is treated within the generalized gradient approximation (GGA) using the Perdew-Burke-Ernzerhof (PBE) functional form. The Grimme method is employed to correct long-range interactions between molecular crystals or substrates and gas molecules. A 5×5×1 supercell is chosen to simulate a monolayer graphene with a 2 nm vacuum layer added in the z-direction. The plane-wave cutoff energy is set to 575 eV. For geometry optimization and electronic structure calculations, k-point grids of 3×3×1 and 6×6×1 are used, and the self-consistent field convergence criterion is 5×10^{-7} eV. Furthermore, the Sorption module employs the grand canonical Monte Carlo (GCMC) method to simulate the adsorption of gaseous molecules on graphene under high-temperature fixed gas pressure conditions. A 14×14×1 supercell is selected to simulate a monolayer graphene with a 3 nm vacuum layer added in the z-

direction. Metropolis algorithm is used for sampling, along with the Universal force field and Ewald method. The charge portion uses QEq, the equilibrium step is set to 1×10^6, and the precision is set to Ultra-fine.

Using water or volatile liquids for ultrasonic dispersion of micro/nano particles/fibers. Preparing materials such as Al_2O_3, SiO_2, amino-functionalized carbon nanotubes, carboxyl-functionalized carbon nanotubes, graphene, amino-functionalized graphene, carboxyl-functionalized graphene, and ferrites in solution. Using methods such as mechanical grinding, high-temperature treatment, acid-base modification, hydrothermal modification, and plasma treatment to functionalize the surface of materials. The molten salt method is used for $FeCl_3$ intercalated graphite, and the H_2O_2 exfoliation method is used to prepare graphene by exfoliating the $FeCl_3$ interlayers. Assembling micro/nano particles with metal conductive grids to construct capillary network channels. Purchasing commercial metal foams and cutting them into curved surfaces closely combined with external metal barrels. Using electric welding to curve the external metal barrel.

Using transmission electron microscope and scanning electron microscope to determine material structure information. Using electrostatic testers, micro and nano ammeters, multimeters, digital oscilloscopes to test current, voltage, open circuit voltage, short circuit current, and using titration method to measure ion content.

As shown in Figure 1a, under the action of an external electric field, Cl^- and Na^+ in the aqueous solution move to the two sides. The electrodes do not contact the solution, quickly dividing the aqueous solution into two parts. In theory, a solution with a single type of net charge can be obtained, which does not violate the laws of charge conservation and other physical and chemical laws. This simple model has not appeared in textbooks or academic research at various levels, and the lack of theoretical research has not provided a definitive answer to whether high-concentration charged solutions exist. After preparing a solution with a single type of charge, whether it can exist stably, the state of the microscopic ions, and the limit of charge it can withstand are all unknown. Referring to the charge distribution in a metal conductor under electrostatic equilibrium, where charges can only distribute on the surface and exist stably, as shown in Figure 1b, a charged solution should also tend to be stable under the effects of Coulomb repulsion within an acceptable range. Ions/charges/charged particles are distributed within the atomic-scale thickness layer on the surface of the liquid. The

corresponding scale can introduce concepts and research content related to forces, magnetism, optics, sound, heat, electricity, superconductivity, and chemistry in multiple research areas such as quantum size effects and topological insulators. Meanwhile, due to the fluidity of the solution, charged solutions exhibit unique physical and chemical properties and have diverse applications. For example, in "strange metals," electricity flows like water, contradicting the fundamental assumption of metal behavior proposed by Lev Landau's Fermi liquid theory [16]. The electrical properties of "strange metals" have long puzzled quantum physicists, unable to explain why charges seem to "dissolve" inside "strange metals." The flow of high-concentration charged solutions into capillary/nano-conductive network structures composed of hydrovoltaic materials with opposite electrical properties can be seen as a higher-scale model of "strange metals," or it may enhance people's understanding of "strange metals," leading to a reassessment of how charges are carried and the discovery of novel experimental phenomena and laws.

The single electrostatic method utilizes electrostatic plates (electrostatic plates in Figure 2 can be removed, placed here for easier understanding) to generate an initial electrostatic field, causing a difference in the distribution of positive and negative ions near the outlets on both sides. Under the influence of gravity, water droplets near the outlets carrying corresponding ions are forced to fall and pass through the hollow conductive rings, dropping into different metal buckets. The metal buckets are connected to the opposite hollow conductive rings via wires to form equipotential bodies. As one side of the metal bucket continuously accumulates charges by receiving either anions or cations, more of the same charges are generated by the opposite hollow conductive ring, resulting in an increasingly strong electrostatic force acting on the top solution, attracting more water droplets containing ions of opposite polarity to fall. At this point, the electrostatic effect generated by the hollow conductive ring is far stronger than the initial electrostatic field generated by the electrostatic plate. This positive feedback mechanism [17-18] exponentially increases the number of corresponding positive and negative ions in the metal buckets on both sides, forming a charged solution. However, the volume of the metal buckets in the single electrostatic method (bottom of Figure 2) is limited, unable to accommodate more charged solutions, and the entire process terminates once the metal buckets are filled with water.

3. Results and Discussion

The designed dual electrostatic method has initially achieved effective separation of anions and cations in the solution (Figure 2, electrostatic attraction, gravity coercion), employing a strategy to remove water while retaining charges (Figure 3, electrostatic repulsion, hydroelectric separation). Based on the principle of electrostatic repulsion (Figure 3a, no charges exist inside equipotential bodies), ions of the same charge in the charged solution are forced to expand outward, causing relatively fewer ions to flow out of the export, creating space, while more charged water droplets enter from the entrance increasing the total charge of the charged solution, thus achieving water's penetration power generation, crucially obtaining the ability to continuously replenish charges. High-concentration charged solutions can be prepared within a minute, achieving a static voltage of 27,000 volts. As shown in Figures 3c-d, a metal foam is used as the base, and the interior of the metal bottle is filled with stainless-steel meshes with an average pore size of 0.03 millimeters, forming a simple water and electricity separation network. Water can continuously flow in and out, with an average voltage of around 22,000 volts (Figure 3b). The sustained emission of high voltage lays the foundation for overcoming application bottlenecks.

Experimental Video: https://www.bilibili.com/video/BV1DZ4y1J7Uj/?spm_id_from=333.999.0.0&vd_source=d1aa9b9c9480b62215fc589302004419

Experimental video: https://www.bilibili.com/video/BV1RA4m157Nz/?spm_id_from=333.337.search-card.all.click&vd_source=d1aa9b9c9480b62215fc589302004419

However, the current structure of our makeshift device considers too few influencing factors and has yet to reach its voltage limit. The material selection, structural design, and stability of charge accumulation in the water and electricity separation zone (i.e., the electrostatic repulsion zone/charge accumulation zone), as well as the overall architecture of the device, urgently need optimization. We have multiple proposals from various angles (force, charge distribution, splash prevention, internal and external interference, constrained pipelines, equipotential body segmentation, high-pressure jetting mechanisms, reflow and reseparation mechanisms, ePTFE phase change dewatering mechanisms, extraction of central liquids, etc.) to improve it. For example, in the future, we plan to optimize the design based on the structure shown in Figure 3b. The conductive plate encasing the water and electricity separation network will have high curvature tips, capable of supporting a high

charge surface density and facilitating charge export (power output). Meanwhile, the water export will be located at the gentle small curvature arc top. The small curvature results in a lower charge surface density, and the arc top position generally leans toward the interior compared to the bottom tip and its nearby area, favoring charge movement to the exterior and the bottom tip position. Additionally, the water export aperture should be made as small as possible while controlling the water inflow and outflow rates to avoid carrying away a large amount of charge with the outflowing water, affecting the charge accumulation efficiency of the high-concentration charged solution. When exploring the limit voltage of high-concentration charged solutions, it may be considered to install high-voltage insulating rings to separate the export from the conductive plate and the conductive network, with the voltage of the high-voltage insulating ring higher than that of the charged solution to repel ions near the outlet to stay inside, while water molecules can flow out freely. However, in practical applications such as desalination and purification processes, the self-generated voltage (over 1000 volts) from the stainless-steel mesh structure far exceeds the reference value for electrodialysis desalination (10-36 volts), so there is no need to install high-voltage insulation waterproof rings to pursue the limit voltage.

As shown in Figure 4a, a metal basin containing a charged solution was detached from the preparation apparatus and left exposed to air, while the electrostatic voltage was measured at a distance using an electrostatic voltmeter (SIMCO FMX-004). Starting at 6200 V, the voltage decreased to 3600 V after 60 s, 970 V after 300 s, and 370 V after 600 s. The charged solution remained stable in the air, maintaining a relatively high voltage within 1 minute. Placing it in a sealed space filled with gases of similar charge (e.g., negative ion air) or common pressure gases like nitrogen or neon (even simply covering it with a hood can deplete the charge in the limited volume of air), may significantly delayed the decline in voltage. As a reference, the Van de Graaff generator ("raging hair" electrostatic ball) takes several minutes to tens of minutes to discharge after stopping operation in air. In air, the voltage of a solid-state Van de Graaff generator can reach 5 million volts, while thunderclouds (gaseous or mixed state, composed of water, ice crystals, and air) range from tens of millions to billions of volts. What is the voltage limit for high-concentration charged solutions (liquid state)? With the ions/charges/charged particles remaining at the liquid surface within a solid container, can the liquid withstand significant electrostatic repulsion with the assistance of the solid container? Is there an insurmountable theoretical limit to the voltage? From a theoretical perspective,

electrostatic repulsion greater than surface tension would tear the liquid apart. However, when a charged solution is stored in a solid container, the solid container can bear all/part/some/one or more directions of the electric field repulsion, not subject to Rayleigh's limit. Therefore, the upper voltage limit of a chargedsolution should approach that of the solid, offering tremendous potential for enhancement. Figure 4b depicts the phenomenon of "electrostatic boiling" that we predict to exist, along with its underlying principles. A charged solution is contained within insulating walls, with the solution drawn from the center and protective inert gas introduced at the top. As the concentration of charged ions increases, the electrostatic force gradually strengthens. When the electrostatic repulsion exceeds the surface tension, the solution surface is torn apart, resulting in the "boiling" phenomenon.

In pure ice, the strong hydrogen bonding between water molecules forms an ordered lattice structure, making ion movement within the ice difficult. Saltwater ice is almost non-conductive because chloride and sodium ions are bound and cannot move freely (Fig. 5a). "Charged solution" is produced by treating low-temperature or supercooled water solution through dual electrostatic method, and after electrostatic equilibrium, it is frozen in liquid nitrogen or a refrigerator to obtain "charged ice crystals" (Fig. 5b). Ions cannot move within solid ice, but can move freely in liquid water. After ions are expanded and positioned, freezing is implemented, and the surface of the ice crystal becomes a single electrical charge. This "solid-liquid transition" can prepare "topological ice crystals." Based on the unique electronic structure of "topological ice crystals," the conductivity, electric field distribution, potential difference, dielectric properties, electrostatic effects, electrical breakdown, refraction, and scattering behavior of ice crystals will all undergo changes. Contrary to expectations, our study of ion-doped ice surfaces revealed that the band gap of quasi-two-dimensional pure ice is 0.138 eV, while that of charged quasi-two-dimensional ice is 3.526 eV (Fig. 5c-f).

The existence of ice in two-dimensional limits has been experimentally verified by Chinese scientists in recent years, and this type of two-dimensional ice is termed "2D Ice I phase". However, specific research regarding its conductivity lacks definitive information in current literature, necessitating further investigation for clarification. Ice itself is an insulator and does not conduct electricity. However, when ice is two-dimensionalized, its physical and chemical properties may undergo alterations, including conductivity. Nevertheless, current research on the conductivity of 2D ice remains insufficient for conclusive outcomes. Significant discrepancies exist in the numerical

values of band gaps among few-layer to multi-layer configurations, different exposed facets, various modes of charge doping, and distinct structural arrangements (as illustrated in Fig. 6c). The asymmetrical and non-equilibrium configurations of elements, orientations (Fig. 6a), arrangements, charges, electric fields, magnetic fields, and force fields (Fig. 6b) can unravel the "Pandora's box" of the "strange ice crystals", presenting infinite possibilities.

As shown in Figure 7a, the voltage limit for preparing charged solutions using the positive feedback dual electrostatic method is explored from various aspects including force interactions, charge distribution, splash prevention, internal and external interferences, constraining channels, potential division in regions, high-pressure jetting mechanisms, and ePTFE phase transition water removal mechanisms. If positive hydrovoltaic materials (such as amino-functionalized carbon nanotubes) and negative charged hydrovoltaic materials (such as carboxyl-functionalized carbon nanotubes) are assembled into a concrete structure with metal conductive grids separately, when water falls into the water and electricity separation network, the surface of the amino-functionalized carbon nanotubes becomes positively charged upon contact with water. The freely mobile negative charges ionized out move downward with the water droplets and exit through the water outlet. Consequently, the water and electricity separation network where the amino-functionalized carbon nanotubes are located exhibits an overall positive charge. Induced positive charges are observed on the interconnected hollow conductive rings, causing the negative charges in the water tank to be attracted to the opposite (Similarly, carboxyl-functionalized carbon nanotubes can induce negative charges on the hollow conductive rings, attracting positive charges in the water tank to the other side). The water and electricity separation network with positive amino-functionalized carbon nanotubes receives positive water droplets, while the water and electricity separation network with negative carboxyl-functionalized carbon nanotubes receives negative water droplets, forming a positive feedback loop, which is enhanced. After the charged water droplets enter the water and electricity separation network and fully contact the conductive grids, according to the principle of electrostatic repulsion, countless moments of motion are considered as a static equilibrium state, where charges can only exist on the surface of the conductor, and charges move towards the surroundings of the water and electricity separation network. Since the water and electricity separation network itself carries fixed positive or

negative charges, the movable positive/negative charges will experience additional electrostatic repulsion from the fixed positive/negative charges, accelerating towards the edges.

Periodic structures with electric charge, such as gratings, photonic crystals, or periodically arranged nanostructures, have the ability to control light. These structures can modulate, focus, deflect, filter, and convert frequencies of light by manipulating physical processes such as interference, diffraction, and scattering. In charged photonic crystals, the distribution of charges can modulate the refractive index of the crystal, affecting the propagation path of light within the crystal (Figure 7b). "Charged ice crystals," "topological ice crystals," "conductive ice crystals," and "strange ice crystals" can provide new avenues and possibilities for the principles research and practical applications of related physicochemical processes such as topological conductors, electro-optical effects, optoelectronic devices, optical communication, optical sensing, optical imaging, fluorescence labeling, quantum structure fabrication, and even lithography and superconductivity fields. The research in this paper can provide "charged solutions" of specific elements. The movement of frozen ions is constrained, and alternating freezing and stacking of charged solutions with anions/cations (Figure 7c) can construct periodic structures with several molecular-level thicknesses (Figure 7f-g), exhibiting semiconductor properties (Figure 7e).

As shown in Figure 8a-b, the surface of the original copper foil used for growing graphene (CVD method) is flat and glossy, exhibiting excellent conductivity and ductility, making it suitable for use as a conductive container wall. We rapidly prepared sheet-like, three-dimensional, rod-like, and hollow cubic structured CuCl crystal materials on the surface of the copper foil using a copper chloride solution at the solid-liquid interface (Figure 8d), obtaining ultra-thin CuCl sheet-like crystals with only a few nanometers in thickness (Figure 8e). This was achieved without any catalysts or additional conditions; simply dripping the copper chloride solution onto the copper foil surface resulted in an instantaneous reaction, transforming the glossy and shiny surface of the copper foil into a rough, earthy yellow color (Figure 8a). Initially, during the preparation of graphene, the applicant used $FeCl_3$ to corrode the copper substrate to obtain various CuCl crystals. However, only the preparation conditions and characterization results were recorded (CrystEngComm, 2016, 18, 3340-3342) [19], without a thorough analysis of the formation mechanism. Currently, there is an opportunity to combine the method in this paper with the following approaches: (1) Utilizing the positive feedback

dual electrostatic method to separate $CuCl_2$ solution, with one side having an excess of Cu^{2+} ions and the other side having an excess of Cl^- ions. Copper can act as the container wall or be inserted into the charged solution, where $Cu + CuCl_2 = 2CuCl\downarrow$, which can be used to eliminate incompletely separated Cu^{2+} ions in the solution and prepare pure Cl^- charged solutions for subsequent research; (2) The key component $FeCl_3$ in the original experiment contains Cl^- and Fe^{3+} ions, while the charged solution contains an excess of either Cl^- or Cu^{2+}. Based on the method of this paper, the effects of Cl^- and Cu^{2+} ions on the growth of CuCl crystals at the interface can be investigated separately, enriching the morphology and exploring the mechanism. In the Cu^{2+} ion-excessive charged solution, Cu^{2+} may play a role similar to Fe^{3+}; (3) Constructing solution models and using acquired theoretical calculation tools and knowledge of crystal growth for in-depth research. The method presented in this paper offers specific multi-ion interfaces, which provide unique advantages for enriching crystal morphology and studying crystal formation mechanisms.

As shown in Figure 9a, the seawater/saline water inflow adopts a zigzag path in the ion separation tube configured to enhance the flow and electrostatic interaction time of the solution. Due to the electrostatic attraction of the electrostatic plates (lasting from a few minutes to several hours), the anions and cations respectively flow to one side. At the bottom layer of the ion separation tube, there are three outlets: the two sides are the outlet of primary ionized water, which flows out of the anion and cation solution respectively, and the deionized water outlet in the middle, which extends to the next saline water tank for another electrostatic separation step (similar to traditional electrophoresis process, but self-powered and with high voltage). Below the outlet of the deionized water, a cylindrical extended electrostatic separation duct with a turbine is set, with the turbine placed inside the extended electrostatic separation duct (for potential energy recovery). The external electrostatic plates of the extended electrostatic separation duct and turbine serve to stabilize and attract static electricity. When the charged water enters the extended electrostatic separation duct, it experiences repulsion from its own static charge, causing the charge to move towards the periphery (self-propulsion). The external electrostatic plates have opposite charges, further causing ions to accumulate at the edges, enabling decentralized separation in the spiral-shaped duct. The secondary ion water tanks store anions and cations separately. By connecting the electrostatic plates on both sides of the ion separation tube with lead-out wires, a positive feedback loop is formed. The

exponentially increasing charged ions in the secondary ion water tanks lead to a sharp increase in the electrostatic voltage on both sides of the ion separation tubes. Setting up multiple stages of ion separation tubes can further improve the desalination efficiency. The above model utilizes the dual electrostatic method of electrostatic attraction and repulsion, as well as positive feedback mechanisms, to generate a strong electric field, facilitating the efficient separation of anions and cations to prepare high-concentration charged solutions and pure water, thereby further increasing the desalination rate. Utilizing wind power, photovoltaics, and other technologies for pumped storage can absorb the wasted wind and solar energy, enabling the in-situ production of pure water, etc., in offshore locations.

The use of stainless steel meshes have enabled water penetrable power generation, aiding in the potential energy recovery and desalination, thus providing a theoretical feasibility for the concept of "seawater for land." As shown in Figure 9b, the average elevation of Yancheng City is less than 5 meters, and the average elevation of Beijing is 43.71 meters, making the "seawater for land" project comparatively less challenging. Referencing the phase one of the South-to-North Water Diversion Project, water is pumped from the Huangjinxia intake at a rate of 70 cubic meters per second into a tunnel 119 meters above water level, achieving a full course of natural flow. Taking Yancheng as an example, by utilizing photovoltaic and wind power for water pumping and storage, seawater can be elevated to a height of 30 meters, creating a height difference with the land of Yancheng. The transportation pipeline gently slopes down towards the land, with a decline of 0.5-1 meter per kilometer set for the pipeline inclination. Each section of the transportation pipeline, being 1 kilometer in length, allows the seawater to naturally flow within it. Electrostatic plates are installed on both sides of the pipeline, with power generation, diversion nodes and concentrated saltwater pipelines set between adjacent transportation pipelines. The power generation and diversion node have a height difference of 1 meter, with water tanks for clean water and brine at the upper end. Demineralized water can directly flow forward along the slope, while water in the brine tank flows down through hollow metal barrels into the water and electricity separation area. Stainless steel mesh serves as the conductive framework for the water and electricity separation network, with wires crossing to connect the two water and electricity separation networks and the hollow conductive ring, forming a positive feedback circuit. This mechanism provides voltage to the hollow metal rings and the electrostatic plates on both sides of the transportation pipeline, converting gravitational potential energy into

electrical energy. Beneath the center of the water and electricity separation network is the demineralized water pipeline, with the concentrated saltwater pipeline at the edge. Water with fewer ions flows out from the demineralized water pipeline into the next transportation pipeline to continue forward, while water with a high ion concentration flows out from the concentrated saltwater pipeline, participating in potential energy recovery and the salt-making process. After passing through ten sections of transportation pipelines and repeatedly separating salt ions, the seawater's salinity decreases to the range of freshwater, with the concentrated brine used for salt production, allowing seawater to advance 10 kilometers inland, achieving "seawater for land." Beijing, more than 100 kilometers from the coastline, can further elevate the water to a height of 60 meters, thereafter eliminating the need for power generation diversion nodes, and directly allowing it to flow into the city. Long-distance, slow movement benefits the efficiency of electrostatic attraction in desalination, as well as facilitates multi-stage desalination, self-power generation, self-flow, self-purification, and salt production.

What are the special properties of high-concentration charged solutions? The Hall effect is known as the queen of solid-state transport experiments. Magnetic fields can not only play a role in the preparation of high-concentration charged solutions but can also be combined with prepared solutions to explore related laws: (1) A magnetic field can induce directional polarization of water's dipole molecules, leading to changes in the electron cloud, which in turn causes bending and local breakage of hydrogen bonds. This results in the single-molecule movement of water, increasing the diffusion coefficient and decreasing viscosity. This is beneficial for the migration and conversion of ions in aqueous solutions, improving mass transfer conditions and thus enhancing the effect of electro-adsorption; (2) A magnetic field can affect the magnetic force couple of salt molecules or ions in water, altering the hydration state of ions in the solution. This change in hydration state modifies the solubility of salts in water, eliminating the affinity (crystallinity) between salt molecules and preventing the crystallization of large crystals; (3) Moving charged particles in a magnetic field experience Lorentz force. Factors such as the direction and intensity of the magnetic field, and the integration of the magnetic field with the electric field, have research value for the synergistic removal of ions from water. They provide conditions for the occurrence of anomalous Hall effect (isopotential body dual-state carrier anomalous Hall effect) and may increase hydrovoltaic conversion efficiency by

10 times; (4) Short-term exposure to a magnetic field can act as a "catalyst" to change the activation energy of water systems, overcoming energy barriers; (5) The Hall effect and the anomalous Hall effect have obvious experimental phenomena, widespread applications, mature and simple detection methods, and reliable results; (6) Based on the establishment of a stable experimental apparatus and a precise law foundation, future research can further attempt to combine hydrovoltaic materials with capillary structures to construct high-scale versions of "strange metal" channels.

In non-magnetic metals or semiconductor materials, electrons (or holes) driven by an electric field (E) undergo deflection due to the Lorentz force under a magnetic field (B) perpendicular to the direction of current. This results in a potential difference (V_H) perpendicular to the plane formed by the electric and magnetic fields, causing electron (or hole) accumulation on the surface of the sample in that direction. This phenomenon is known as the Hall effect (Figure 10a). However, the presence of a magnetic field is not a necessary condition for the Hall effect. The anomalous Hall effect occurs without an external magnetic field (B) deflecting the electron's trajectory due to the ordered arrangement of spontaneous magnetization magnetic moments (M) in magnetic materials (Figure 10b). Near the Fermi surface, the number of spin-up and spin-down electrons is unequal. When an electric field (E) is applied, spin-up and spin-down electrons deflect in opposite directions due to spin-related scattering and spin-orbit coupling, resulting in spin polarization (spin current) and a potential difference (V_H) at the interfaces. Gravitation drives ion-containing water flow through a permanent magnetic water and electricity separation network structure with abundant capillary channels. The permanent magnetic water and electricity separation network structure acts as an external magnetic field source for each capillary water flow (consistent with the normal Hall effect), causing directional separation of liquid carriers (Na^+ or Cl^-). Countless capillary water flows with the same charge in ferromagnetic materials are equivalent to countless currents. Many capillary water flows have statistically significant directional flow, acting on the permanent magnet as a whole, meeting the conditions for triggering the anomalous Hall effect, causing solid-state carriers to appear at both ends. As shown in Figure 10d, compared to traditional Hall effect and anomalous Hall effect, the integrated bipolar carriers in the magnet channel represent a combination carrier of statistically significant Hall effect and anomalous Hall effect, meeting the conditions for simultaneously triggering both effects. The voltage values formed by the liquid carriers and solid-state carriers should be approximately ten

times that of the normal Hall effect. As shown in Figures 10e-f, using a magnetizer to magnetize ferromagnetic materials in a directed manner generates an outward magnetic field perpendicular to the paper surface. Placing electrodes, voltmeters, and ammeters at corresponding positions enables the detection of whether the Hall effect and anomalous Hall effect occur simultaneously.

4. Conclusion

The innovations of this article can be summarized as follows: (1) The establishment of a technique for preparing high-concentration charged solutions using a dual electrostatic feedback method. This method employs electrostatic attraction, gravity separation, and positive feedback mechanisms to effectively separate anions and cations in the solution. Through electrostatic repulsion and the use of a permissive electrostatic separation network, the partitioning of homoelectric ions is achieved, allowing continuous replenishment of single-charge species, crucially enabling sustained power generation; (2) The identification of evidence for the existence of charged solutions/high-concentration charged solutions and the prediction of electrostatic boiling phenomena, enriching the field of electrostatics and electrochemistry research; (3) Proposal of exploring the limit voltage of high-concentration charged solutions from multiple angles including force effects, charge distribution, splash prevention, internal and external interferences, constrained pipe flow, partitioning of equipotential bodies, high-pressure jetting mechanisms, reflow and re-separation mechanisms, and ePTFE phase transition water removal mechanisms; (4) Introduction of the unique topological and physicochemical properties of charged solutions/high-concentration charged solutions and prediction of anomalous Hall effect of dual-state charge carriers in equipotential bodies; (5) Proposal of a self-powered desalination technology based on dual electrostatic methods, combined with technologies such as wind power, photovoltaics, and pumped storage, to mitigate the waste and intermittency of wind and solar power and promote the desalination of seawater for land use; (6) Introduction of concepts such as charged ice crystals, topological ice crystals, conductive ice crystals, and strange ice crystals, along with their preparation and application prospects; (7) Proposal of the application prospects of charged solutions in the fields of water splitting and crystal synthesis.

This article introduces a newly established research field with extensive content, requiring fine-tuned research and improvement. It is hoped that this work will provide inspiration to both the

academic and industrial sectors, satisfying the author’s pursuit of truth. Any inadequacies in the text are open to criticism and correction.

ACKNOWLEDGEMENTS

The author gratefully acknowledges support from Natural Science Foundation of Jiangsu Province for Young Scientists (Grant No. BK20201064).

References

[1] X. Xu, X. Zhu, J. Zhou, R. Li. *Exploration of desalinating synthetic seawater through an electrophoresis technology featuring vertical electric field*. CIESC Journal, 2015, 66(S2): 332-341.

[2] J. Yin, W. Guo. *Review: the rise of hydrovoltaics*. JHIT, 2020, 27(3): 20-25.

[3] S. Yang, M. Chen, Y. Su, J. Xu, X. Wu, C. Tian, *Stabilization of hydroxide ions at the interface of a hydrophobic monolayer on water via reduced proton transfer*. Phys. Rev. Lett. 2020, 125(15): 156803.

[4] X. Yu, Y. Zhang, R. Hu, X. Luo, *Water droplet bouncing dynamics*. Nano Energy 2021, 81: 105647.

[5] L. Li, Z. Zheng, C. Ge, Y. Wang, H. Dai, L. Li, S. Wang, Q. Gao, M. Liu, F. Sun, T. Zhang, *A flexible tough hydrovoltaic coating for wearable sensing electronics*. Adv. Mater. 2023, 35, (40): 2304099.

[6] S. Chaurasia, R. Kumar, T. Tabrizizadeh, G. Liu, K. Stamplecoskie, *All-weather-compatible hydrovoltaic cells based on Al_2O_3 TLC Plates*. ACS Omega 2022, 7(3): 2618-2623.

[7] C. Zheng, W. Chu, S. Fang, J. Tan, X. Wang, W. Guo, *Materials for evaporation-driven hydrovoltaic technology*. Interdiscip. Mater. 2022, 1(4):449-470.

[8] J. Yin, Z. Zhang, X. Li, J. Yu, J. Zhou, Y. Chen, W. Guo, *Waving potential in graphene*. Nat. Commun. 2014, 5: 3582.

[9] J. Yin, X. Li, J. Yu, Z. Zhang, J. Zhou, W. Guo, *Generating electricity by moving a droplet of ionic liquid along graphene*. Nat. Nanotechnol. 2014, 9(5): 378-383.

[10] G. Xue, Y. Xu, T. Ding, J. Li, J. Yin, W. Fei, Y. Cao, J. Yu, L. Yuan, L. Gong, J. Chen, S. Deng, J. Zhou, W. Guo, *Water-evaporation-induced electricity with nanostructured carbon materials*. Nat. Nanotechnol. 2017, 12(4): 317-321.

[11] W. Xu, H. Zheng, Y. Liu, X. Zhou, C. Zhang, Y. Song, X. Deng, M. Leung, Z. Yang, R. X. Xu, Z. Wang, X. Zeng, Z. Wang, *A droplet-based electricity generator with high instantaneous power density*. Nature 2020, 578: 392-396.

[12] Y. Lu, S. Song, R. Wang, Z. Liu, J. Meng, A. J. Sweetman, A. Jenkins, R. C. Ferrier, H. Li, W. Luo, T. Wang, *Impacts of soil and water pollution on food safety and health risks in China.* Environ. Int. 2015, 77: 5-15.

[13] A. Azizullah, M. N. K. Khattak, P. Richter, D. P. Hader, *Water pollution in Pakistan and its impact on public health—A review*. Environ. Int. 2011, 37(2): 479-497.

[14] L. Bao, K. A. Maruya, S. A. Snyder, E. Y. Zeng, *China's water pollution by persistent organic pollutants.* Environ. Pollut. 2012, 163: 100-108.

[15] B. C. Hodges, E. L. Cates, J. H. Kim, *Challenges and prospects of advanced oxidation water treatment processes using catalytic nanomaterials*. Nat. Nanotechnol. 2018, 13(8): 642-650.

[16] L. Chen, D. Lowder, E. Bakali, A. Andrews, W. Schrenk, M. Waas, R. Svagera, G. Eguchi, L. Prochaska, Y. Wang, C. Setty, S. Sur, Q. Si, S. Paschen, D. Natelson, *Shot noise in a strange metal*. Science 2023, 382: 907-911.

[17] H. Huang, *Voltage build-up time responses of Kelvin's water droplet generator: Variations due to different geometric configurations*. J. Electrostat., 2014, 72(6): 447-456.

[18] G. Planinsic, T. Prosen, *Conducting rod on the axis of a charged ring: The Kelvin water drop generator*. Am. J. Phys., 2000, 68(12): 1084-1089.

[19] Z. Miao, M. Liang, Z. Xiao, B. Amir, X. Li, L. Zhi. *Cations-induced fast growth of ultrathin cuprous chloride nanoplatelets*. CrystEngComm, 2016, 18, 3340-3342.

SUPPORTING INFORMASTION

Using alcohol lamp wick mesh with an aperture of approximately 3 mm overlaid to form the water and electricity separation conductive grid (Figure S1a), tin foil wrapped around plastic cups are used as the hollow conductive ring and electrodes for the water and electricity separation zone. With the electroscope's probe opened, a voltage of 5 V can be measured (Figure S2). The reason for the low voltage is that the water flow rate is high, the mesh grid's aperture is large, and the entire circular surface of the bottom alcohol lamp wick mesh is not covered, allowing water to leak from both the edge and central areas. The water quickly flows out without sufficient contact with the conductive network, causing water droplets to be in an elevated state as they flow out from the bottom of the metal grid, carrying away a large amount of charge, resulting in insufficient voltage attracted by the upper conductive ring due to electrostatic attraction. However, the experimental results indicate the feasibility of water-permeable power generation, which is the most fundamental verification of all the research in this article.

Copper plates are welded into barrels, with a layer of metal foam nickel with an aperture of approximately 0.3 mm welded at the bottom of the barrel (Figure S1b), with a thickness of 100 mm. Once water starts flowing, the suspended small ball near the conductive ring swings, indicating a relatively high voltage. A static voltage of 1000-5000 V is measured (Figure S2). The experimental results demonstrate the successful realization of water-permeable power generation by the water and electricity separation network, with voltage values meeting the requirements of some applications. However, the thickness of the metal foam nickel is too thin, resulting in high costs and limited charge storage capacity.

Building upon the previous experimental setup, a significant amount of stainless steel braided mesh with an aperture of approximately 0.03 mm is filled into the metal barrel (Figure S1c). Upon the initiation of water flow, intense vibrations of the suspended small ball occur, yielding a static voltage of 10,000-27,000 V (Figure S2), achieving highly desirable results. The experimental outcomes drive towards even higher voltage limits.

Experimental video: https://www.bilibili.com/video/BV1RA4m157Nz/?spm_id_from=333.337.search-card.all.click&vd_source=d1aa9b9c9480b62215fc589302004419

Based on the dual electrostatic water drop generator and LC resonance, the export, storage, and emission of charges can be achieved, leading to the transmission of radio waves. The charge at the tip continuously charges the capacitor, and the increasing voltage causes the spark gap to break down, forming a circuit. The capacitor charges the inductor coil, forming LC resonance. Due to the continuous charging and discharging of the inductor, electromagnetic waves are generated and released into the surrounding space. The oscillation frequency and electromagnetic wave frequency can be regulated by adjusting the parameters of the inductor and capacitor in the LC circuit (Figure S3). The dual electrostatic water drop generator's capability to export, store, and emit charges, as well as transmit radio waves, has potential applications in the field of wireless charging.

Experimental video: https://www.bilibili.com/video/BV1oK41187XN/?spm_id_from=333.999.0.0)

The positive and negative hydrovoltaic materials are assembled with a conductive network for "concrete" construction, serving as water and electricity separation zones (Figure S4m), facilitating positive feedback acceleration and strengthening electrostatic repulsion, while also filling voids to control water flow rates. Factors affecting the system performance of positive and negative hydrovoltaic materials include the quantity of ionized charges, types of ionized ions, conductivity, particle size, and content ratio of the materials.

The adsorption properties of H_2O molecules on graphene, Janus-graphene, SiO_2 (111) surface, and Al_2O_3 (1-12) surface were calculated using the grand canonical Monte Carlo method under conditions of 298 K and 100 kPa (Figure S4a-l). There is a significant difference in the adsorption quantity of H_2O molecules on both sides of Janus-graphene, with the oxygen-containing group side having significantly more adsorption. The adsorption properties of H_2O molecules on SiO_2 and Al_2O_3 surfaces are not prominent, suggesting surface functionalization to enhance adsorption capacity and fixed charge formation.

The zero charge point refers to the point where the ζ potential of the solid surface is zero. If the charged state of the solid surface is related to the pH of the solution, there must be a pH value at which the solid surface charge is zero. As shown in Figure S4n, the zero charge point of Al_2O_3 corresponds to a solution pH of approximately 9, with Al_2O_3 positively charged at pH < 9 and negatively charged at pH > 9; the zero charge point of SiO_2 corresponds to a solution pH of 2.5, with SiO_2 positively charged at pH < 2.5 and negatively charged at pH > 2.5. Based on the zero charge point division rule, the selection range of positive and negative hydrovoltaic material combinations can be greatly expanded, facilitating the realization of efficient and cost-effective new materials and devices.

Furthermore, the mobile positive and negative charges in the aqueous solution not only come from the H^+ and OH^- ions ionized from H_2O but also include Na^+, K^+, Cl^-, C3H7COO$^-$, C8H17COO$^-$, solute particles, etc. The movement speed of conducting ions in the solution differs, with H^+, OH^-, Na^+, K^+, and Cl^- reacting more rapidly under the action of an electric field compared to $C_3H_7COO^-$, $C_8H_{17}COO^-$, solute particles, etc. (Figure S4o), which can serve as one of the criteria for comparing various material performances.

The density of states (DOS) diagrams for monolayer graphene, bilayer graphene, $FeCl_3$-intercalated bilayer graphene ($FeCl_3$-bilayer graphene), and Janus graphene with epoxy groups on one side (Janus-graphene) were calculated using first-principles methods (Figure S5a). The valence and conduction bands of graphene, bilayer graphene, and $FeCl_3$-bilayer graphene intersect, exhibiting metallic properties. The DOS of $FeCl_3$-bilayer graphene at the Fermi level is two orders of magnitude higher than that of graphene and bilayer graphene, indicating that the intercalation of $FeCl_3$ enhances the conductivity of bilayer graphene (the conductivity is proportional to the DOS at the Fermi level). This is likely due to the increased carrier concentration caused by $FeCl_3$ intercalation. Figure S5b shows the absorption coefficient of the four materials. Visible light corresponds to frequencies ranging from 3.84×10^{14} Hz to 7.7×10^{14} Hz (1.6 eV-3.2 eV), marked with light pink bars. The intercalation of $FeCl_3$ has a negligible effect on the

absorption coefficient of graphene, and transparency in the visible light region even improves. This provides material options for finding non-metallic, waterproof, corrosion-resistant, transparent, and conductive containers, as well as for performing photochemical reactions at the interface of water and electricity separation zones. However, in cases of incomplete exfoliation, $FeCl_3$-bilayer graphene forms interconnected powder structures with various pores (Figure S5d), which can constitute a well-conductive water and electricity separation network and can be mass-produced. The valence and conduction bands of Janus-graphene have a bandgap, with the Fermi level located near the valence band, making it a semiconductor. As shown in Figure S5c, 2-stage $FeCl_3$-graphite intercalation compound ($FeCl_3$-GIC) was prepared by molten salt method, double-layer graphene was obtained by exfoliation using H_2O_2, and $FeCl_3$-bilayer graphene was formed again by $FeCl_3$ intercalation. Figure S5d shows the incompletely exfoliated powder structure. As shown in Figure S5e, using graphite as the raw material, 2-stage $FeCl_3$-GIC was oxidatively intercalated using chlorate and concentrated sulfuric acid. Due to the strong bonding between $FeCl_3$ and graphite layers, preventing the infiltration of concentrated acid and strong oxidants, the original $FeCl_3$ intercalation structure remains intact, but the carbon layer without $FeCl_3$ intercalation is oxidized by concentrated acid, forming a large number of oxygen-containing groups inside the carbon layer, resulting in "heterogeneous alternately intercalated graphite". By selecting mild ultrasonic treatment, the oxygen-containing layer of "heterogeneous alternately intercalated graphite" can be easily peeled off, obtaining "$FeCl_3$-dispersible- graphene". Single-sided selective oxidation of Janus-graphene can be obtained by reacting hydrogen peroxide with ferric chloride, and placing it in water, stirring it, with the hydrophobic side facing upwards contacting the air, and the hydrophilic side downwards contacting the aqueous solution, Janus-graphene materials disperse at the gas-liquid interface, self-assembling into monolayer graphene films (Figure S5f). Janus-graphene films can be used in electrodes and water and electricity separation zones. Placing Janus-graphene in liquid nitrogen for quenching, followed by freeze-drying, can be rolled into quasi-one-dimensional nanoribbons or contracted into three-dimensional granular aggregates. Due

to the asymmetry of Janus-graphene, it is easier to form curved structures from planar structures during cooling (Figure S5g). Janus- graphene, with one side having hydrophilic oxygen-containing groups and the other side being unmodified by oxidation, is a class of materials with special structures, minimal structural damage, and strong controllability, providing advantages in preparing atomic-layer-thick transparent electrodes and constructing water and electricity separation zones.

The material, structure, conductivity, and transparency of the container wall can enrich the application scenarios of charged solutions. For example, a waterproof and corrosion-resistant transparent conductive container can provide special conditions for processes like photocatalytic water splitting at the interface (Figure S6a), while crystal growth can occur on the surface of conductive copper foil, and a flexible, breathable waterproof film can utilize the phase change of water to remove water (Figure S6b). Based on Raoult's law, Dalton's law of partial pressures, and the Clausius-Clapeyron equation describing the relationship between vapor pressure and the concentration of a solution, the inherent hydrophobic effect of the waterproof and breathable layer completely isolates liquid seawater and its salt and other impurity components, allowing only water vapor to diffuse through, as depicted in Figure S6c. There exists a natural vapor pressure difference between seawater and highly water-absorbent resin, which serves as the driving force for mass transfer, enabling the spontaneous migration of moisture from the seawater side, where it vaporizes, diffuses through the membrane, and is absorbed and liquefied on the highly water-absorbent resin side. Using a semi-permeable membrane to encase water-absorbing powder that can be decomposed and utilized by the human body, an osmotic pressure difference exists between the water-absorbing powder and the absorbed highly water-absorbent resin, promoting the transport of water molecules across the semi-permeable membrane to the water-absorbing powder side. After the water-absorbent resin swells, it not only comes into closer contact with the semi-permeable membrane but also increases pressure during its own expansion process, facilitating the transport of water molecules. As shown in Figure S6d, the increment pressure method utilizing the vapor pressure difference and osmotic pressure difference to in-situ prepare potable water from

seawater and wastewater effectively isolates ions and impurities from seawater and wastewater, making it suitable for use in maritime emergencies, wilderness travel, and industrial beverage preparation, among other applications. This method does not require the external high pressures associated with reverse osmosis, thus avoiding the cumbersome decontamination procedures of traditional methods. Experimental results have shown that this design holds potential for entry into everyday life and industrial production, and it also indicates that ePTFE has the ability to remove water while retaining charge, making it a viable option for preparing high-concentration charged solutions.

Figure Legends

Figure 1: (a) Schematic diagram of simple preparation of charged solution, (b) Schematic diagram of ion/charge distribution in charged solution.

Figure 2: Schematic diagram of the single electrostatic method for preparing charged solutions with positive feedback mechanism.

Figure 3: (a) Schematic diagram of electrostatic repulsion principle, (b) Composition of the core part of electrostatic repulsion and voltage measurement results, (c) Voltage and phenomena induced by metal foam, (d) Voltage and phenomena induced by stainless steel braided mesh. The bottom shows four theoretical bases.

Figure 4: (a) Curve of the voltage variation over time for a charged solution existing alone and exposed to air, (b) Prediction of the phenomenon of "electrostatic boiling" and its principle.

Figure 5: (a) Schematic diagram of ice and "topological ice crystals," (b) Schematic diagram of charged ice crystal preparation, (c) Model diagram of quasi-two-dimensional ice, (d) Model diagram of charged quasi-two-dimensional ice, (e) Band structure diagram of quasi-two-dimensional ice, (f) Band structure diagram of charged quasi-two-dimensional ice.

Figure 6: (a) Probability of multiple crystal facets exposed in pure ice crystals, (b) Model diagram of the "strange ice crystal" structure formed by different valence state ferromagnetic ions freezing in ice crystals to create non-equilibrium periodic electric and magnetic fields, (c) Numerical values of band gaps for different crystal orientations, thicknesses, ions, and structures (data being supplemented).

Figure 7: (a) Schematic diagram of the instrument design for preparing high-concentration charged solutions, (b) Ice lens, (c) Schematic diagram of the alternately stacked structure of positive and negative ion layers frozen layer by layer, (d) Top view structure diagram of hexagonal ice phase, (e) Side view structure diagram of hexagonal ice phase, (f) Top view structure diagram of alternately stacked anion/cation ice layers, (g) Side view structure diagram of alternately stacked anion/cation ice layers, (h) Density of states of hexagonal ice phase and alternately stacked layers of ice containing anions and cations, (i) Real and imaginary parts of the dielectric function.

Figure 8: (a) The left half depicts the smooth surface of the original copper foil, while the right half shows a non-reflective rough surface with grown crystals. (b) SEM image of the original copper foil surface. (c) Schematic diagram of non-equilibrium ionic interface reactions. (d) SEM images of four morphologies of CuCl crystal materials. (e) TEM image, elemental surface scan, and optical property image of ultra-thin CuCl sheet-like crystals.

Figure 9: Self-powered desalination and water purification model of positive feedback dual electrostatic method and "seawater for land".

Figure 10: (a) Schematic diagram of the Hall effect, (b) Schematic diagram of the anomalous Hall effect, (c) Schematic diagram of ferromagnetic material structure with capillary channels, (d) Schematic diagram of carrier movement inside ferromagnetic material, (e) Schematic diagram of a droplet-based hydrovoltaic generator with coexisting spontaneous magnetization of magnetic moments and Hydrovoltaic effect, (f) Schematic diagram of test setup for moving charged water droplets inside ferromagnetic materials.

Figure S1: (a)-(c) Corresponding materials and phenomena for the water and electricity separation conductive network with aperture sizes of 3, 0.3, and 0.03 mm.

Figure S2: Corresponding voltage values for the water and electricity separation conductive networks with aperture sizes of 3, 0.3, and 0.03 mm.

Figure S3: Schematic diagram of the structure and principle of the dual electrostatic water drop generator capable of emitting radio waves.

Figure S4: (a)-(d) Top views of graphene, Janus-graphene, SiO_2 (111) surface, and Al_2O_3 (1-12) surface, (e)-(h) Side views of graphene adsorbing H_2O molecules, Janus- graphene adsorbing H_2O molecules, SiO_2 surface adsorbing H_2O molecules, and Al_2O_3 surface adsorbing H_2O molecules, (i)-(l) Side views of the distribution of the center of mass of H_2O molecules on the graphene surface, Janus-graphene surface, SiO_2 surface, and Al_2O_3 surface, all at a temperature of 298 K and a fugacity of 100 kPa, (m) A conductive network for water and electricity separation containing positive and negative hydrovoltaic materials, (n) Schematic diagram of the relationship between the surface chargeability of

Al_2O_3 and SiO_2 materials and the pH of the solution, (o) A table showing the migration speeds of various charged ions in the solution.

Figure S5: (a) Density of states and (b) Absorption coefficient plot of monolayer graphene, bilayer graphene, $FeCl_3$-bilayer graphene and Janus-graphene, (c) Preparation of bilayer graphene and $FeCl_3$-bilayer graphene by H_2O_2 stripping of $FeCl_3$ intercalated graphite, (d) Powder of $FeCl_3$-bilayer graphene, (e) Synthesis of Janus graphene, (f) Interface self-assembly of Janus-graphene thin film, (g) Dimensional variation of Janus-graphene.

Figure S6: (a) Schematic diagram of a transparent conductive electrode for photocatalytic water splitting, (b) Waterproof breathable membrane for phase separation of water, retaining ions and separating water, reducing volume, and increasing concentration, (c) Principle schematic diagram of in-situ preparation of drinking water from seawater and wastewater using the osmotic pressure difference and vapor pressure difference increment pressure method, (d) Diagram of glucose powder wrapped with ePTFE and semipermeable membrane for water absorption and expansion.

Figures

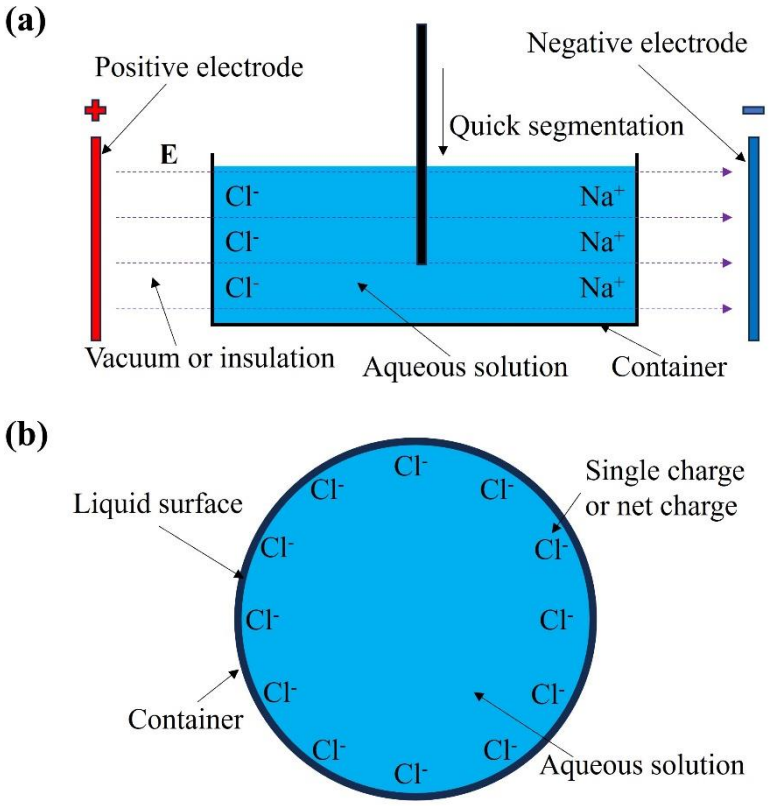

Figure 1

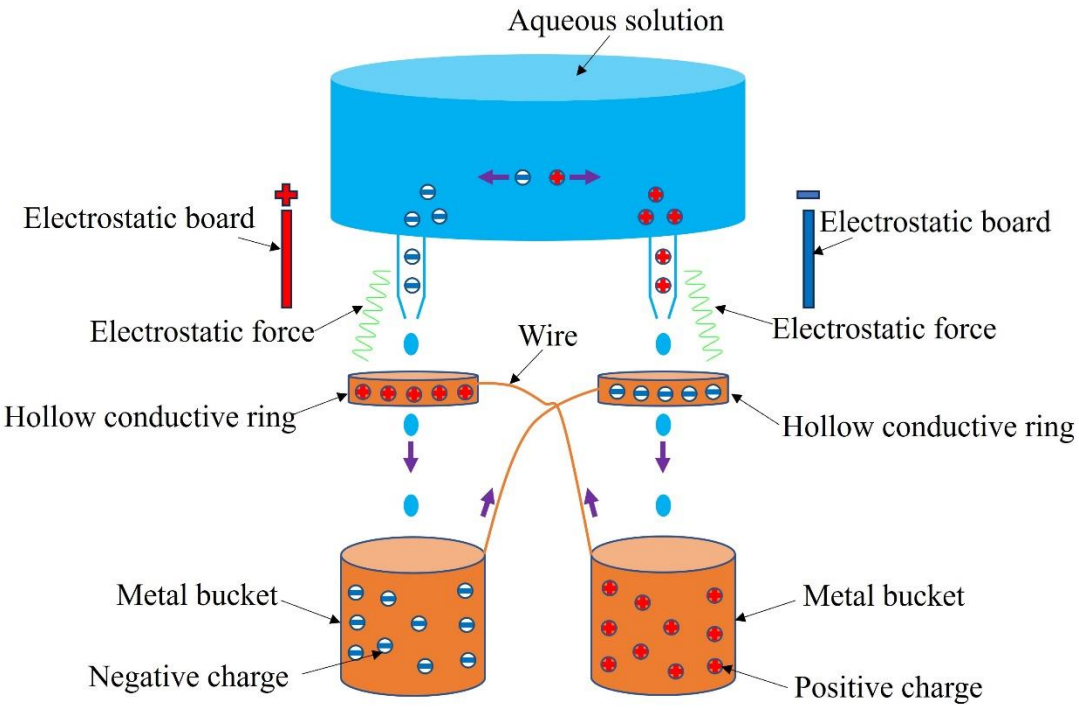
Aqueous solution
Electrostatic board
Electrostatic board
Electrostatic force
Electrostatic force
Wire
Hollow conductive ring
Hollow conductive ring
Metal bucket
Metal bucket
Negative charge
Positive charge

Figure 2

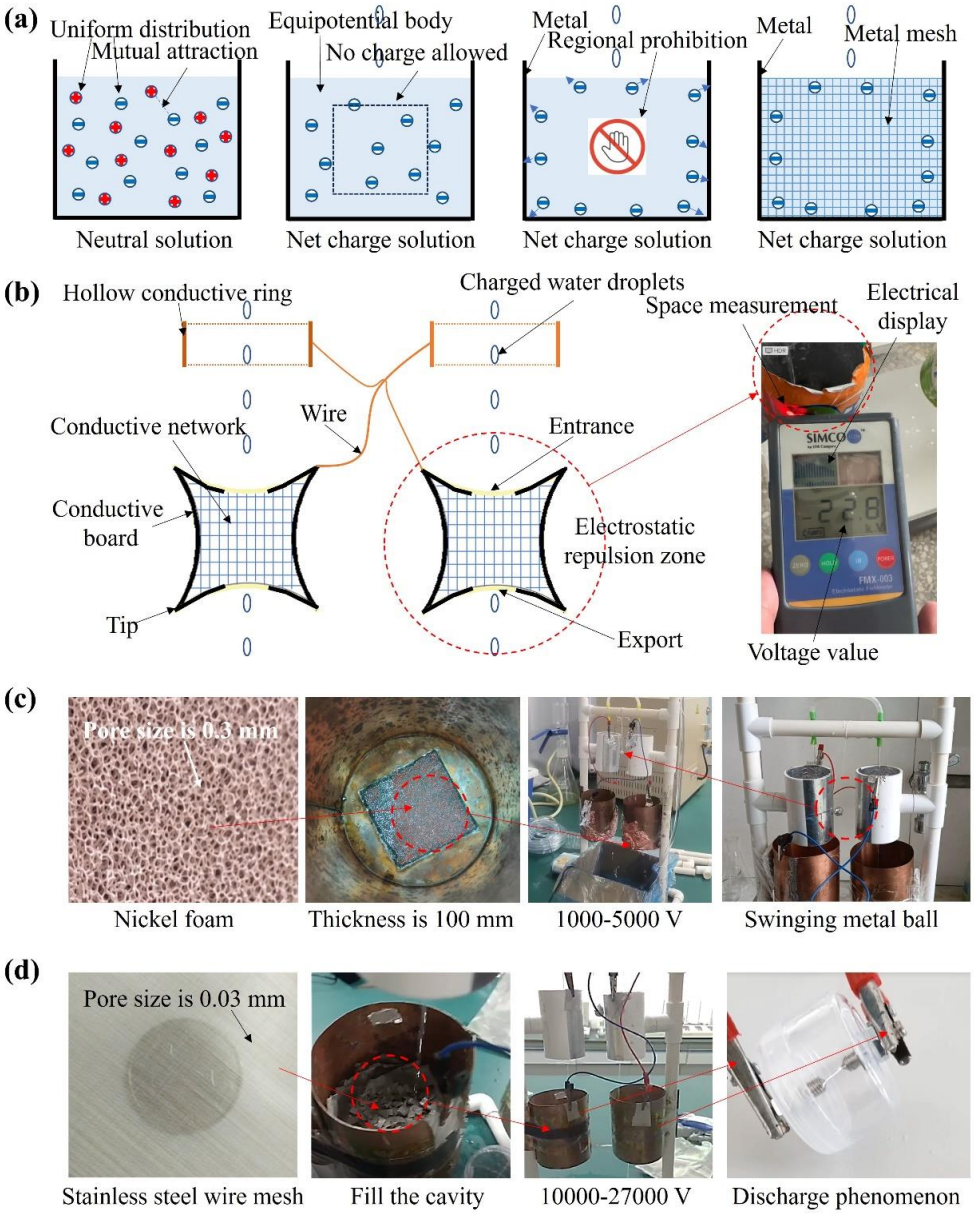

Basis 1: Under the condition of electrostatic equilibrium, the internal charge density of a conductor is always zero (Gaussian theorem)

Basis 2: The direction of motion of the internal charge (non-equilibrium) in a conductor tends towards an electrostatic equilibrium state (the lowest energy)

Basis 3: The metal mesh integrates the solution with the container, metalizes the solution, and quickly tends towards electrostatic equilibrium (The interior of an equipotential body can conduct not only electrons but also single charged ions, forming a unique liquid/solid biphasic carrier system)

Basis 4: Water is an extremely weak electrolyte with very weak conductivity, strong binding ability between OH^- and H^+, and target ions/charges/particles swim towards the outermost layer using water as the medium (the atomic core is fixed in the solid, and the outer electrons swim)

Figure 3

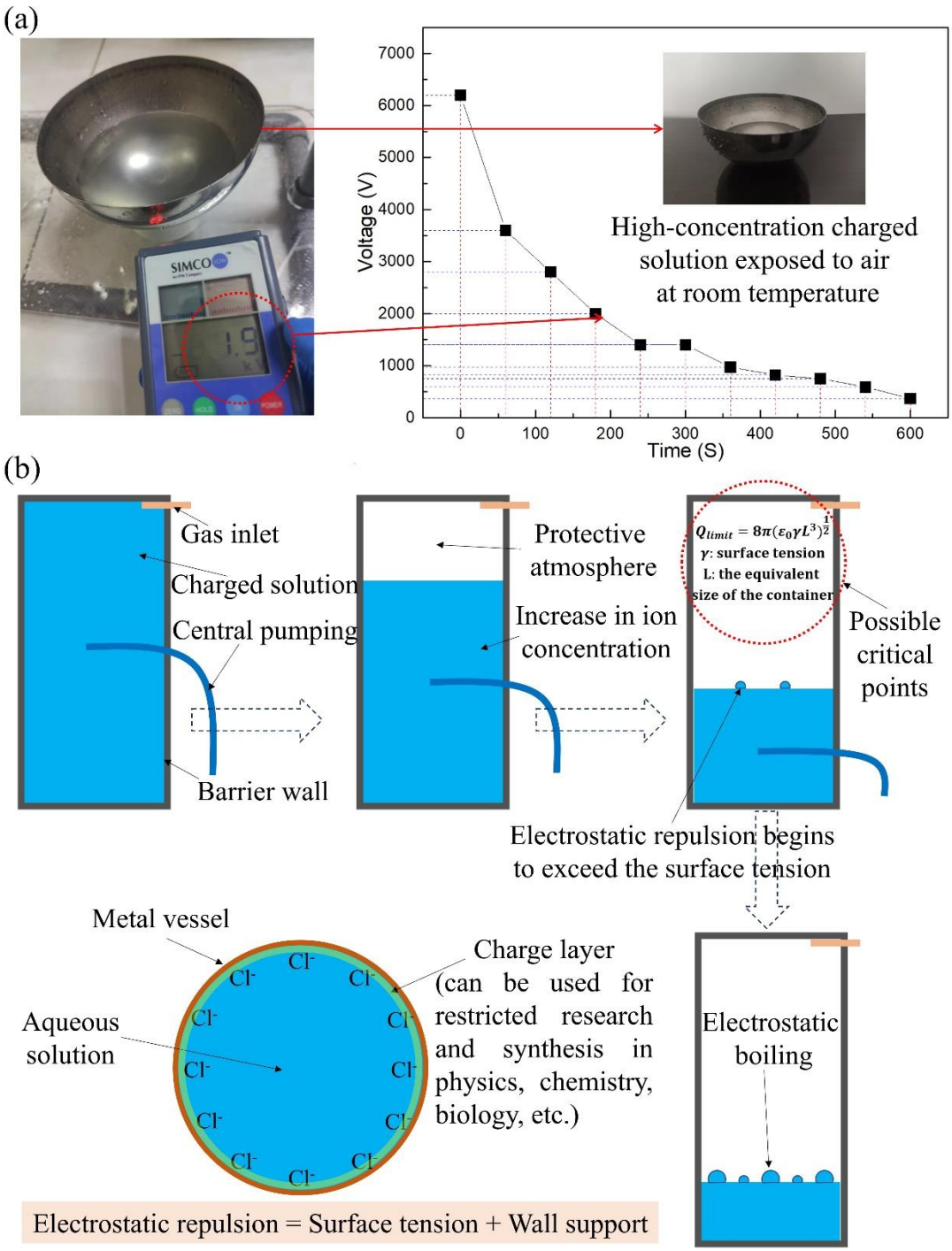
(a)
SIMCO
7000
6000
5000
4000
3000
2000
1000
0
Voltage (V)
0
100
200
300
400
500
600
Time (S)
High-concentration charged solution exposed to air at room temperature
(b)
Gas inlet
Charged solution
Central pumping
Barrier wall
Protective atmosphere
Increase in ion concentration
$Q_{limit} = 8\pi(\varepsilon_0 \gamma L^3)^{\frac{1}{2}}$
γ: surface tension
L: the equivalent size of the container
Possible critical points
Electrostatic repulsion begins to exceed the surface tension
Metal vessel
Aqueous solution
Cl-
Charge layer (can be used for restricted research and synthesis in physics, chemistry, biology, etc.)
Electrostatic boiling
Electrostatic repulsion = Surface tension + Wall support

Figure 4

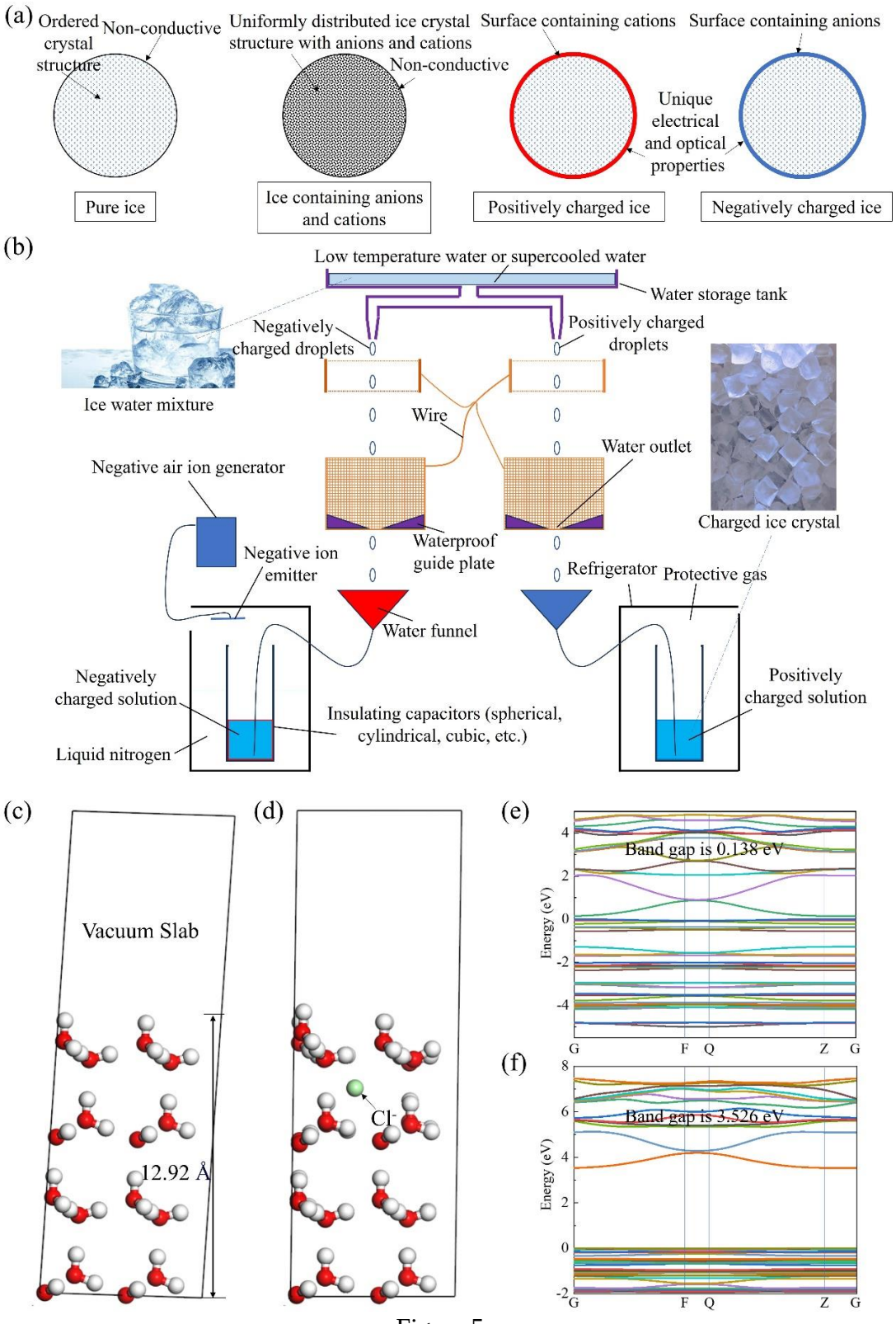
(a)
Ordered crystal structure
Non-conductive
Uniformly distributed ice crystal structure with anions and cations
Non-conductive
Surface containing cations
Surface containing anions
Unique electrical and optical properties
Pure ice
Ice containing anions and cations
Positively charged ice
Negatively charged ice
(b)
Low temperature water or supercooled water
Water storage tank
Negatively charged droplets
Positively charged droplets
Ice water mixture
Wire
Water outlet
Negative air ion generator
Charged ice crystal
Waterproof guide plate
Negative ion emitter
Refrigerator
Protective gas
Water funnel
Negatively charged solution
Insulating capacitors (spherical, cylindrical, cubic, etc.)
Positively charged solution
Liquid nitrogen
(c)
Vacuum Slab
12.92 Å
(d)
Cl-
(e)
Band gap is 0.138 eV
Energy (eV)
G F Q Z G
(f)
Band gap is 3.526 eV
Energy (eV)
G F Q Z G

Figure 5

(a)

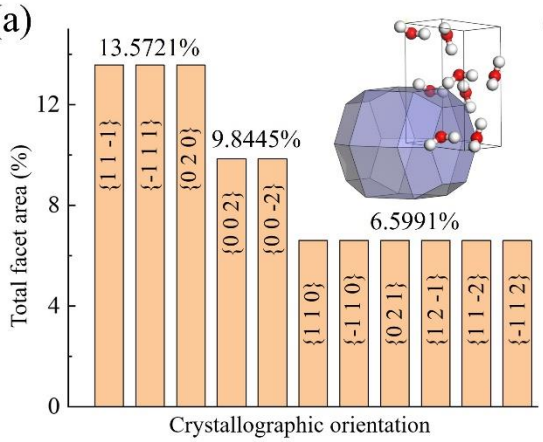

(b)

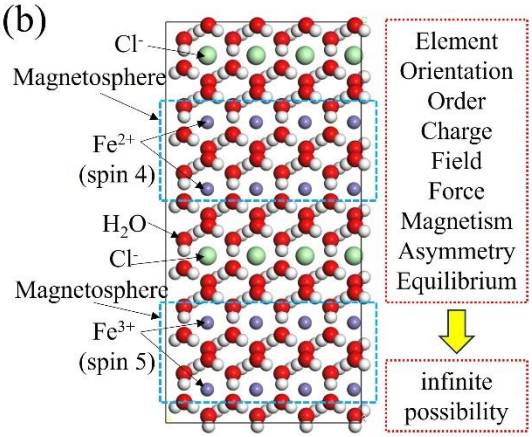

(c)

Thickness (layer) / Band gap (eV) / Crystal orientation	2	3	4	5	6	7	8	9
{1 1 -1}	2.275	0.528	0.026					
{-1 1 1}	2.310							
{0 2 0}								
{0 0 2}	2.798		0.138					
{0 0 -2}	1.191							
{1 1 0}	4.453							
{-1 1 0}	4.503							
{0 2 1}	4.205							
{0 2 -1}	4.111							
{1 1 -2}	4.056							
{-1 1 2}	4.396							
Contain Cl^-			3.526					
Contain Na^+								
Contain Na^+ and Cl^-			2.745					
Other ions								
Alternating structure								
Other structures								

Figure 6

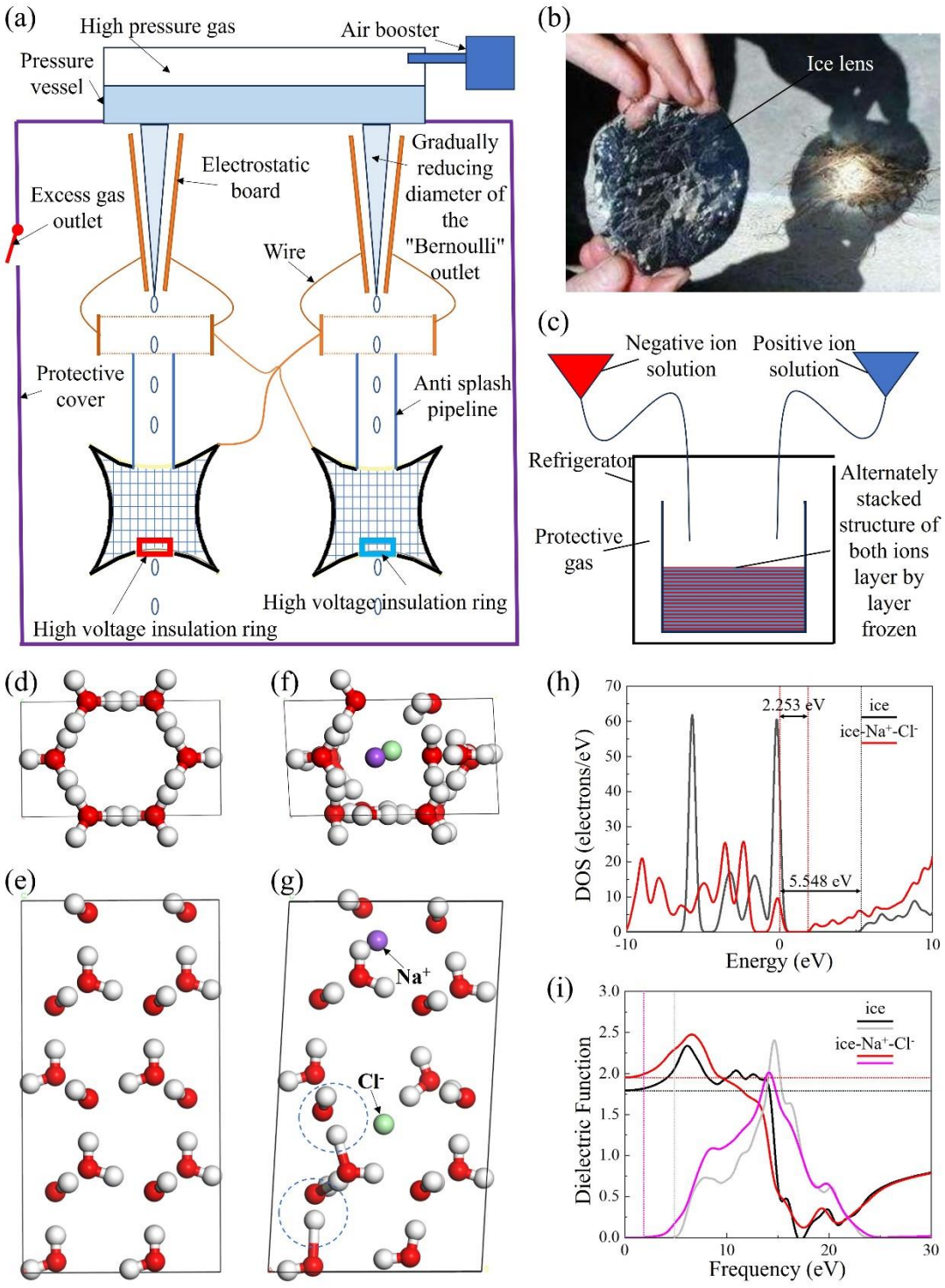
(a)
High pressure gas
Air booster
Pressure vessel
Electrostatic board
Gradually reducing diameter of the "Bernoulli" outlet
Excess gas outlet
Wire
Protective cover
Anti splash pipeline
High voltage insulation ring
High voltage insulation ring
(b)
Ice lens
(c)
Negative ion solution
Positive ion solution
Refrigerator
Protective gas
Alternately stacked structure of both ions layer by layer frozen
(d)
(f)
(e)
(g)
Na+
Cl-
(h)
2.253 eV
ice
ice-Na+-Cl-
5.548 eV
DOS (electrons/eV)
Energy (eV)
(i)
ice
ice-Na+-Cl-
Dielectric Function
Frequency (eV)

Figure 7

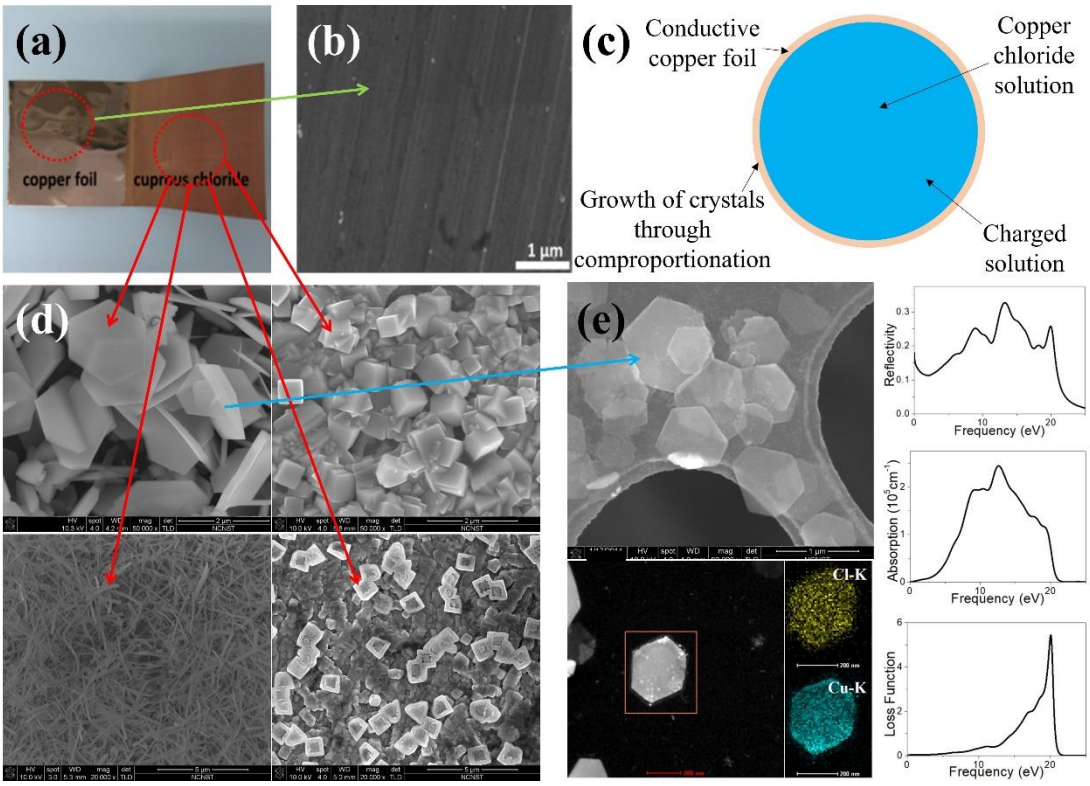
(a)
copper foil
cuprous chloride
(b)
1 μm
(c)
Conductive copper foil
Copper chloride solution
Growth of crystals through comproportionation
Charged solution
(d)
(e)
Cl-K
Cu-K
Reflectivity
Frequency (eV)
Absorption (10^5 cm^-1)
Frequency (eV)
Loss Function
Frequency (eV)

Figure 8

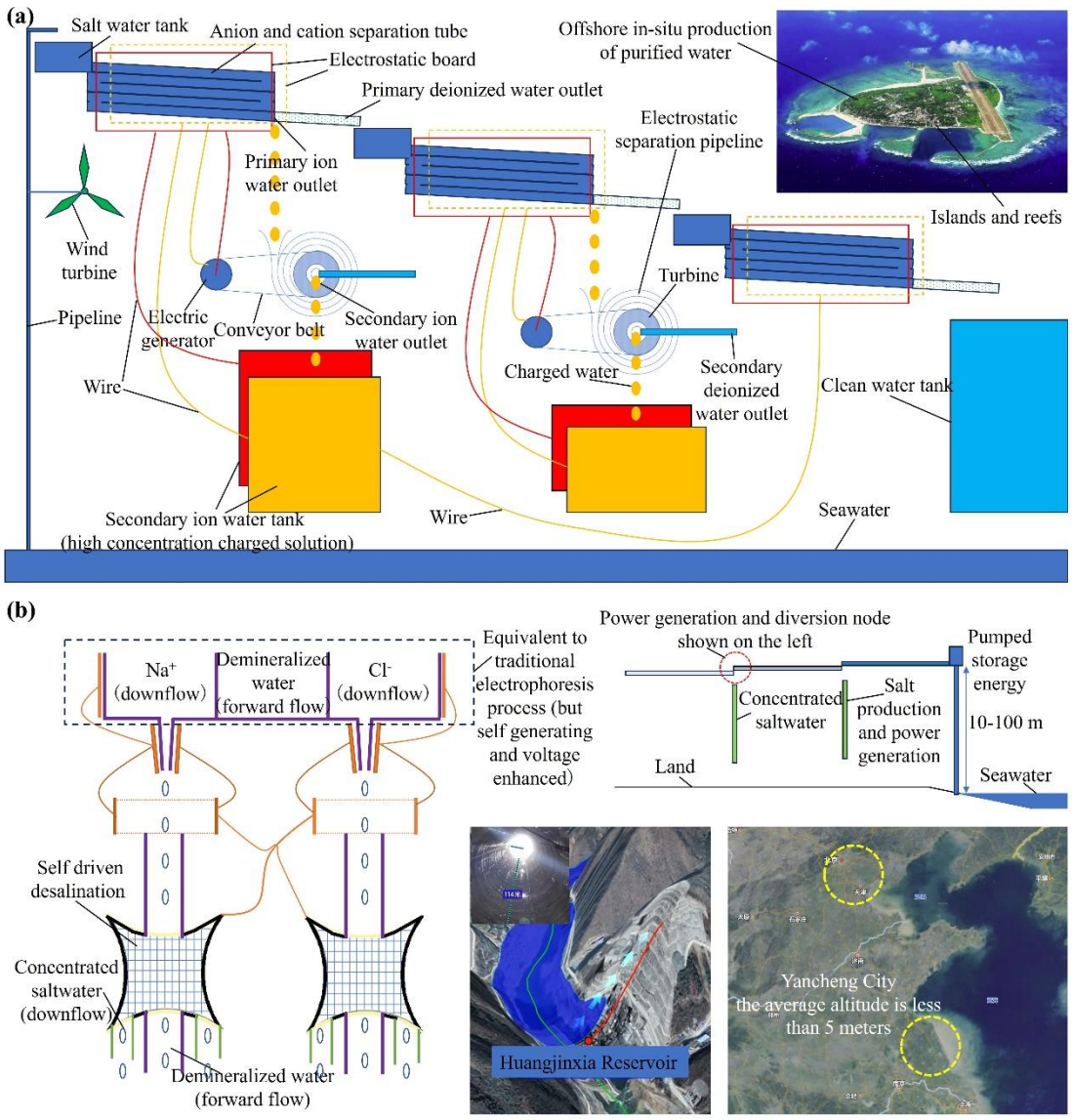
(a)
Salt water tank
Anion and cation separation tube
Electrostatic board
Primary deionized water outlet
Offshore in-situ production of purified water
Electrostatic separation pipeline
Primary ion water outlet
Islands and reefs
Wind turbine
Turbine
Pipeline
Electric generator
Conveyor belt
Secondary ion water outlet
Charged water
Secondary deionized water outlet
Clean water tank
Wire
Secondary ion water tank (high concentration charged solution)
Wire
Seawater
(b)
Na+ (downflow)
Demineralized water (forward flow)
Cl- (downflow)
Equivalent to traditional electrophoresis process (but self generating and voltage enhanced)
Power generation and diversion node shown on the left
Pumped storage energy
Concentrated saltwater
Salt production and power generation
10-100 m
Land
Seawater
Self driven desalination
Concentrated saltwater (downflow)
Demineralized water (forward flow)
Huangjinxia Reservoir
Yancheng City
the average altitude is less than 5 meters

Figure 9

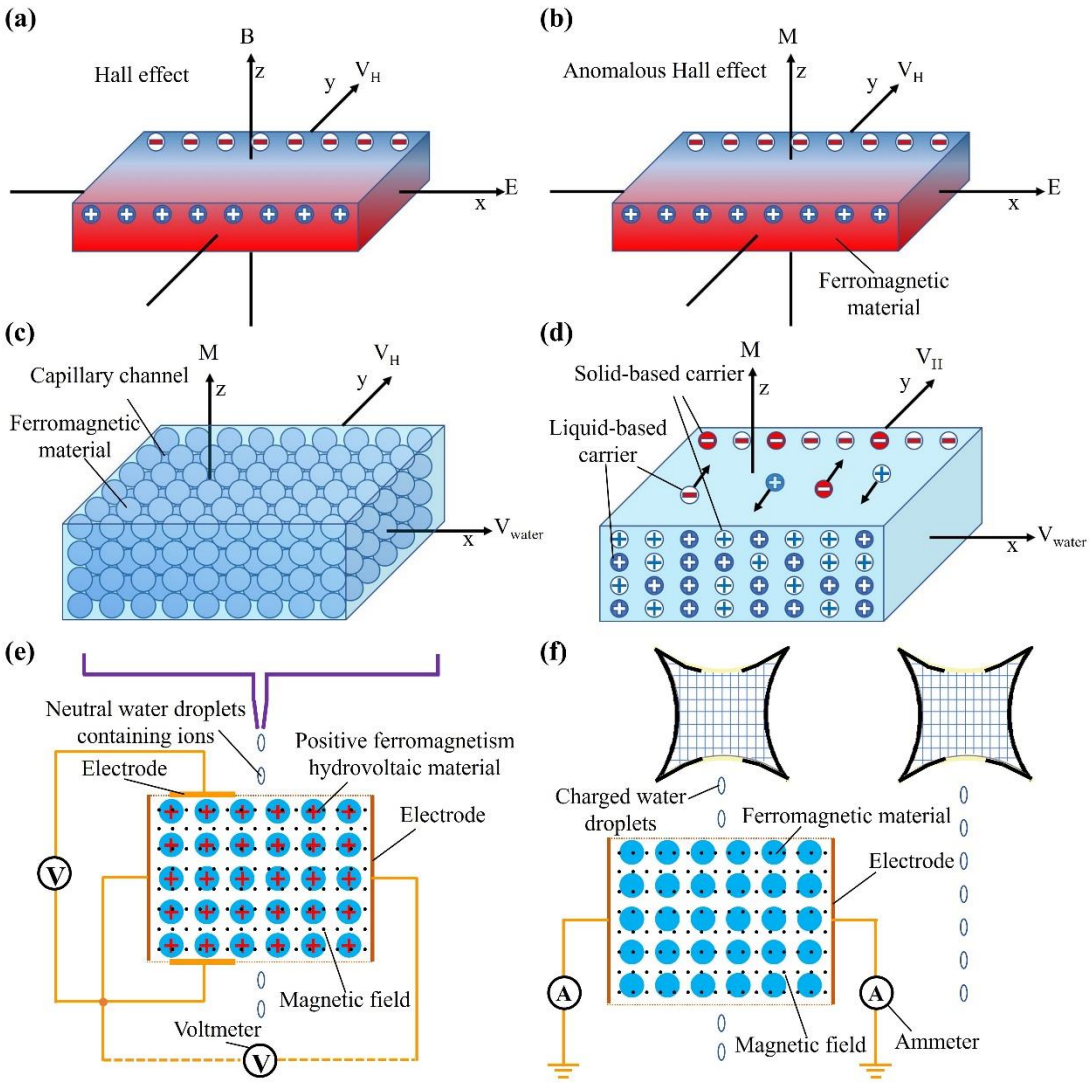
(a)
Hall effect
B
z
y
V_H
E
x
(b)
Anomalous Hall effect
M
z
y
V_H
E
x
Ferromagnetic material
(c)
Capillary channel
Ferromagnetic material
M
z
V_H
y
V_{water}
x
(d)
Solid-based carrier
Liquid-based carrier
M
z
V_{II}
y
V_{water}
x
(e)
Neutral water droplets containing ions
Positive ferromagnetism hydrovoltaic material
Electrode
Electrode
V
Magnetic field
Voltmeter
V
(f)
Charged water droplets
Ferromagnetic material
Electrode
A
A
Magnetic field
Ammeter

Figure 10

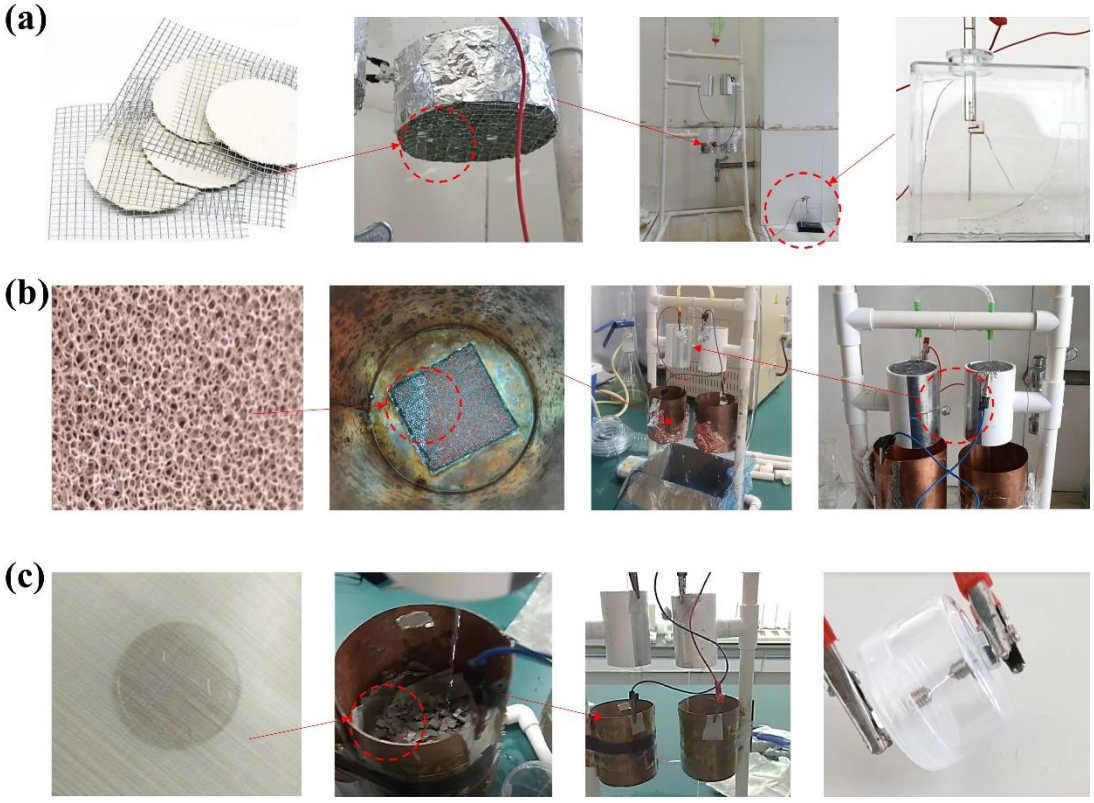

Figure S1

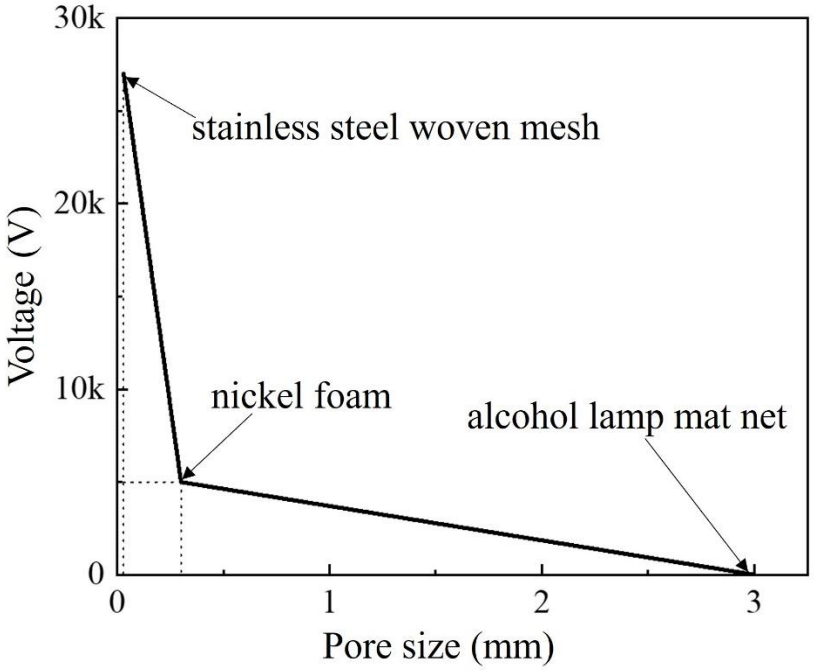
30k
20k
10k
0
Voltage (V)
stainless steel woven mesh
nickel foam
alcohol lamp mat net
0
1
2
3
Pore size (mm)

Figure S2

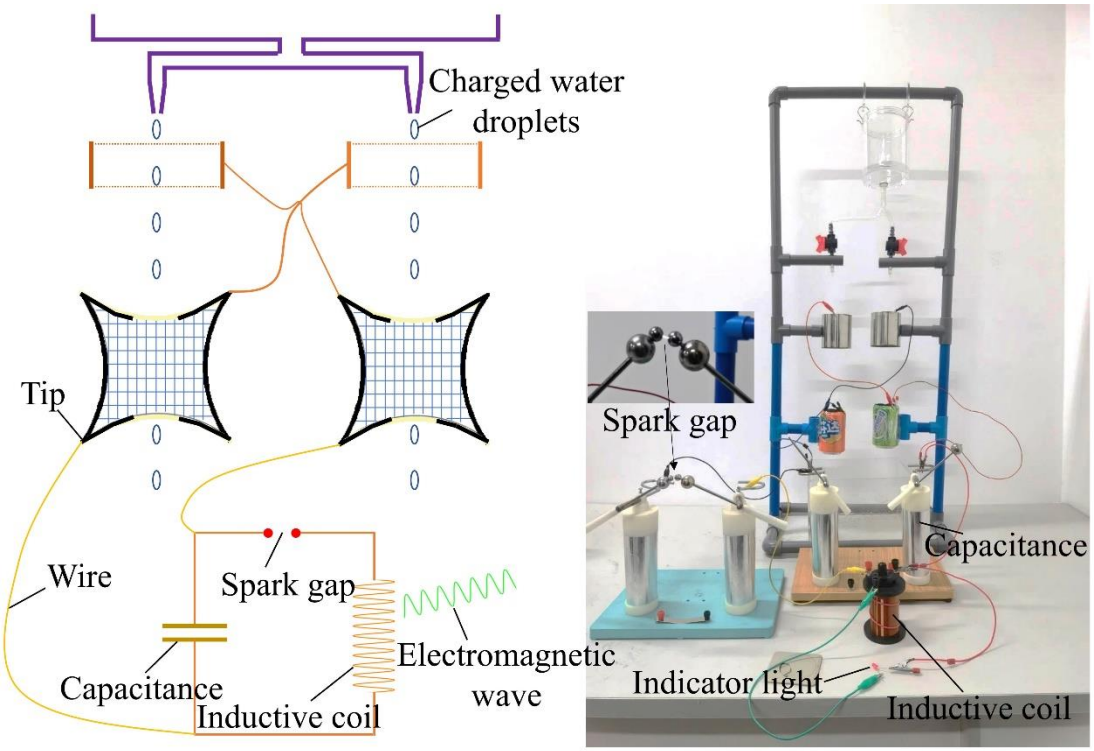
Charged water
droplets
Tip
Wire
Spark gap
Capacitance
Inductive coil
Electromagnetic
wave
Spark gap
Capacitance
Indicator light
Inductive coil

Figure S3

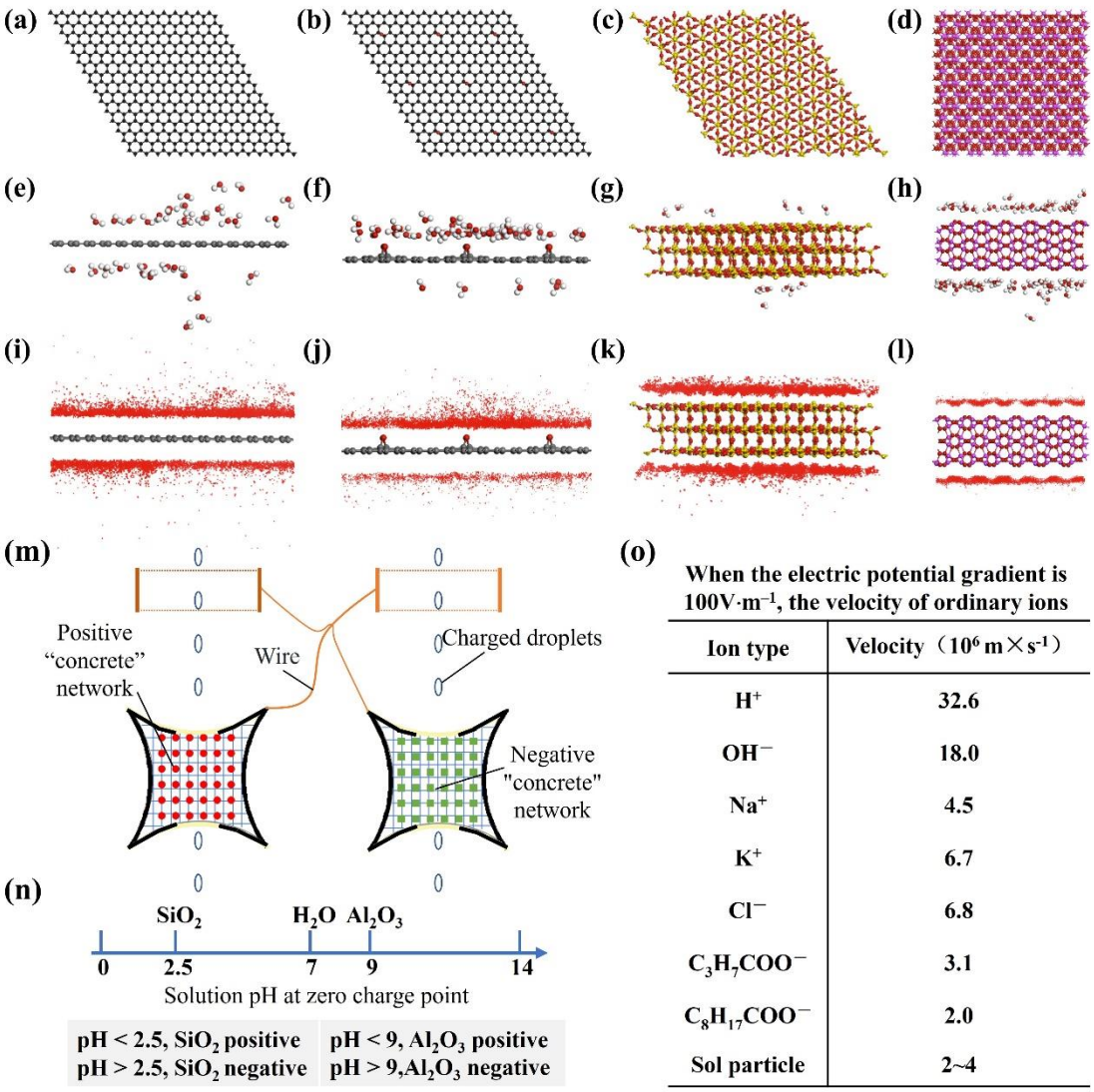

(o)

When the electric potential gradient is 100V·m^{-1}, the velocity of ordinary ions

Ion type	Velocity（10^6 m×s^{-1}）
H^+	32.6
OH^-	18.0
Na^+	4.5
K^+	6.7
Cl^-	6.8
$C_3H_7COO^-$	3.1
$C_8H_{17}COO^-$	2.0
Sol particle	2~4

Figure S4

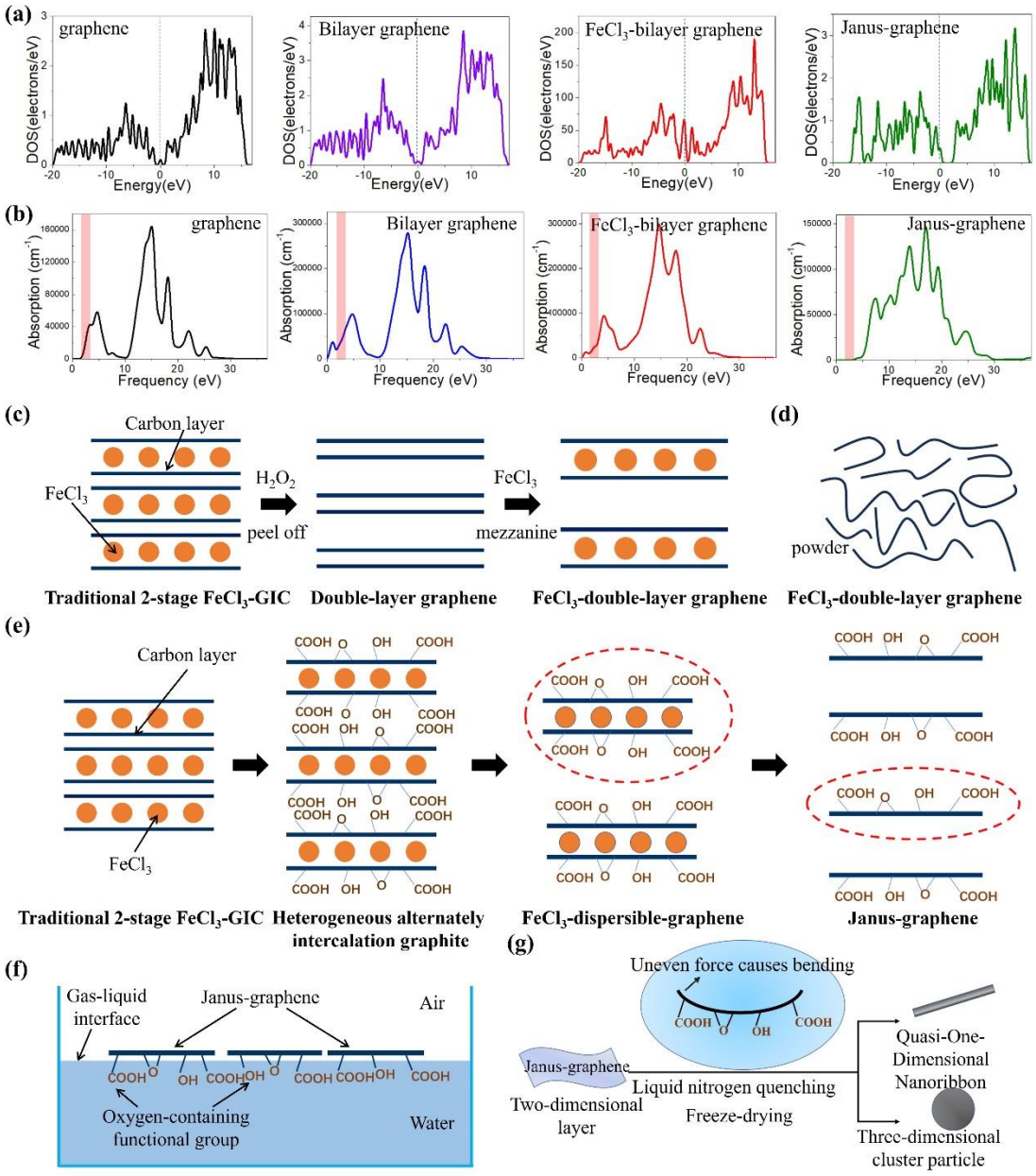
(a)
graphene
Bilayer graphene
FeCl3-bilayer graphene
Janus-graphene
DOS(electrons/eV)
Energy(eV)
(b)
Absorption (cm-1)
Frequency (eV)
(c)
Carbon layer
FeCl3
H2O2
peel off
FeCl3
mezzanine
Traditional 2-stage FeCl3-GIC
Double-layer graphene
FeCl3-double-layer graphene
(d)
powder
FeCl3-double-layer graphene
(e)
Carbon layer
FeCl3
COOH
OH
O
Traditional 2-stage FeCl3-GIC
Heterogeneous alternately intercalation graphite
FeCl3-dispersible-graphene
Janus-graphene
(f)
Gas-liquid interface
Janus-graphene
Air
Water
Oxygen-containing functional group
(g)
Uneven force causes bending
Janus-graphene
Two-dimensional layer
Liquid nitrogen quenching
Freeze-drying
Quasi-One-Dimensional Nanoribbon
Three-dimensional cluster particle

Figure S5

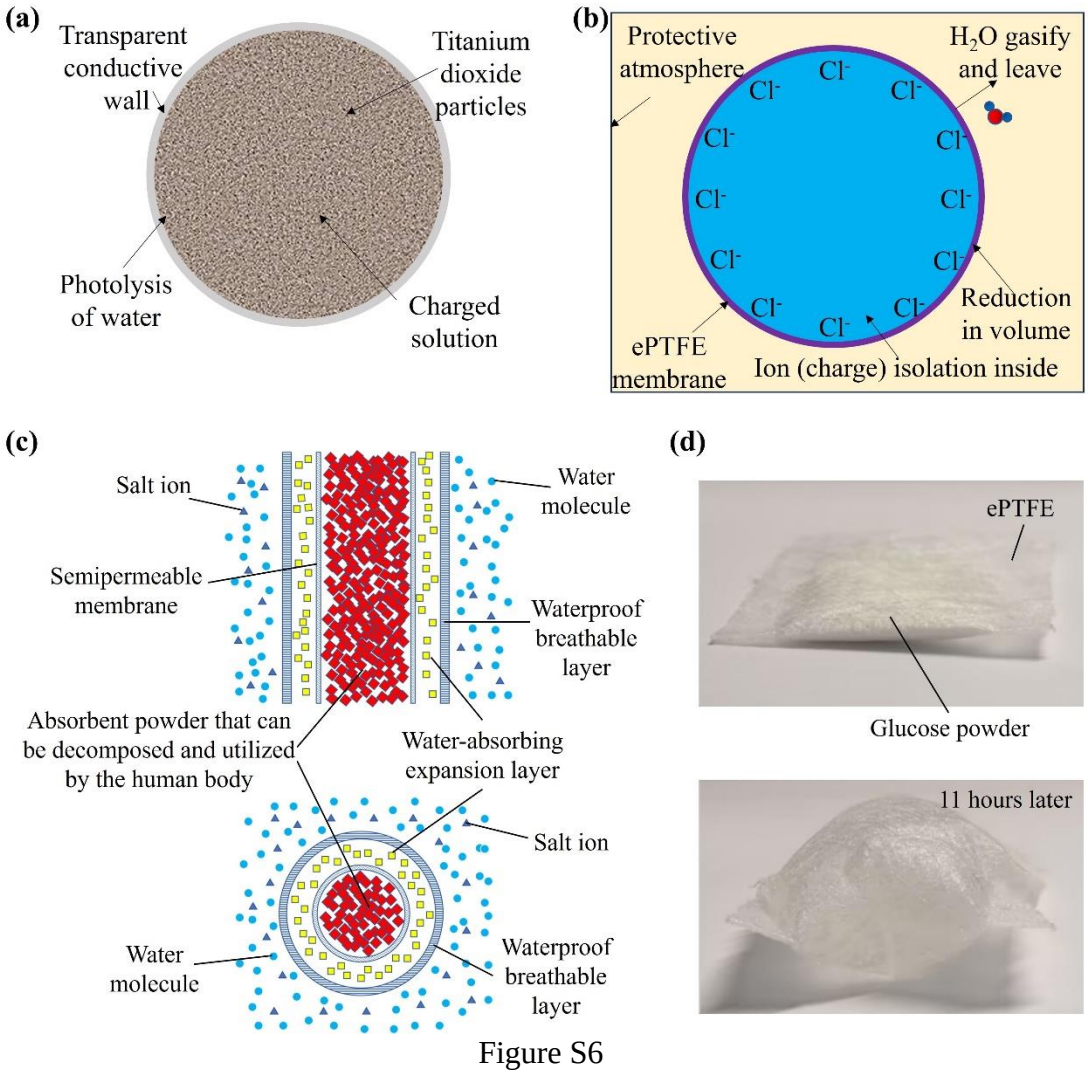
(a)
Transparent conductive wall
Titanium dioxide particles
Photolysis of water
Charged solution
(b)
Protective atmosphere
H_2O gasify and leave
Cl-
Reduction in volume
ePTFE membrane
Ion (charge) isolation inside
(c)
Salt ion
Water molecule
Semipermeable membrane
Waterproof breathable layer
Absorbent powder that can be decomposed and utilized by the human body
Water-absorbing expansion layer
Salt ion
Water molecule
Waterproof breathable layer
(d)
ePTFE
Glucose powder
11 hours later

Figure S6